Physics – Uspekhi **57** (4) 389 – 406 (2014)

100th ANNIVERSARY OF THE BIRTH OF Ya B ZELDOVICH PACS numbers: 52.40.Db, 98.70.Vc, 98.80.Es

CMB spectral distortions during the recombination of the primeval plasma in the early Universe

V G Kurt, N N Shakhvorostova

DOI: 10.3367/UFNe.0184.201404f.0423

Contents

1. **Introduction** 389
   1.1 CMB as a probe of the evolution of the Universe; 1.2 Before and after recombination: a brief history of the Universe
2. **CMB and its properties** 392
   2.1 Discovery of CMB; 2.2 CMB anisotropy; 2.3 Spectral characteristics of CMB
3. **Thermal history of the Universe before the primeval plasma recombination** 393
   3.1 Evolution of matter composition in the early Universe; 3.2 Spectral distortions of CMB during energy release in the early Universe
4. **Recombination of the primeval hydrogen–helium plasma** 395
   4.1 Plasma emission during recombination; 4.2 Physics of recombination of the primeval hydrogen plasma; 4.3 Basic methods of primeval plasma recombination kinetics calculations; 4.4 Recombination of the primeval helium plasma and modern methods of recombination kinetics calculations
5. **CMB spectral distortions during recombination of the primeval plasma** 400
   5.1 Short-wavelength CMB spectral distortions; 5.2 Emission during transitions between higher levels of hydrogen and helium atoms; 5.3 Notes on possible future methods of observations
6. **Conclusion** 404
7. **Appendix. Comparison of primeval plasma recombination emission with nebular emission** 405

References 405

Abstract. **Virtually all physical processes occurring during hydrogen and helium recombination ($900 < z < 7000$) are currently well understood. The theoretical work of the last decade on this topic provides a comprehensive picture of recombination and related processes. Of particular observational interest is the fact that the CMB spectrum experiences a unique distortion from the blackbody spectrum due to the release of photons during this epoch. These additional photons form a cosmological recombination spectrum imposed on the thermal CMB spectrum. The recombination dynamics of hydrogen are controlled by two processes — the two-photon decay 2s → 1s and the L_α photon escape due to multiple scattering in an expanding medium — of which the first is dominant. About 57% of all hydrogen atoms in the Universe at $z \lesssim 1400$ recombined through the two-photon decay channel. Because the ratio of the CMB photon and baryon number densities is extremely large, the additional photons make up only a small fraction ($10^{-8} - 10^{-9}$) of the total number, and hence their distorting effect of the CMB spectrum is small. Of most promise for future observations are relative distortions in the Rayleigh–Jeans range of the CMB spectrum (the decimeter range). For example, at 300 MHz, relative intensity distortions of the order of $10^{-8} - 10^{-9}$ are expected. The Balmer and Paschen hydrogen series fall into the range of a CMB maximum. In the Wien range, observations are greatly hampered — and indeed made impossible — by the infrared and submillimeter cosmic background. Given the current level of instrumentation, it is not yet possible to measure small distortions ($< 10^{-8}$) near the maximum. Some researchers believe, however, that an accuracy of ~ 10 nK can soon be achieved. Because the CMB spectrum does not depend on the direction, any region of the sky can be chosen for observation, preferably so as to minimize the contribution of various cosmic backgrounds and noises (for example, near a galactic pole). It is also essential that the sought signal be nonpolarized in order that it can be separated from signals from other sources.**

V G Kurt, N N Shakhvorostova Astro-Space Center, Lebedev Physical Institute, Russian Academy of Sciences, Leninskii prosp. 53, 119991 Moscow, Russian Federation
E-mail: vkurt@asc.rssi.ru, nadya@asc.rssi.ru

Received 3 March 2014
Uspekhi Fizicheskikh Nauk **184** (4) 423 – 443 (2014)
DOI: 10.3367/UFNr.0184.201404f.0423
Translated by K A Postnov; edited by A M Semikhatov

1. Introduction

1.1 CMB as a probe of the evolution of the Universe

The 20th century was remarkable for the rapid development of cosmology — the science about the structure and evolution of the Universe. Over several decades, this comparatively young theoretical science acquired a solid observational foundation thanks to many balloon and space experiments. It would not be an exaggeration to assert that the modern development of observational instrumentation renders cos-

mology a more and more exact science. It now encompasses not only theoretical concepts on the evolution of the Universe and interpretation of observations but also highly precise measurements of the cosmological parameters. This became possible due to the modern cosmological experiments *WMAP*[1] and *Planck*[2] aimed at studying the cosmic microwave background (CMB) with high accuracy. Because this radiation has been present since the very first seconds of the Universe's history, the modern CMB bears imprints of physical processes that occurred at different stages of the evolution of the Universe.

The so-called standard cosmological model includes the modern picture of the Universe's evolution and the physical processes that occurred at different epochs. This model is heavily based upon CMB temperature anisotropy sky maps, which allow probing matter distribution in the 'pre-galactic' epoch, and upon large catalogs of galaxies, which demonstrate the modern three-dimensional distribution of matter in space (for example, SDSS[3]). Using these data, the known laws of gravitational instability growth allow calculating the primordial spectrum of cosmological perturbations and key cosmological parameters that directly affect the evolution of the perturbations up to the modern large-scale structure formation. For example, the discovery and measurements of the CMB temperature anisotropy evidence that no galaxies were present in the early Universe, and the relative matter density fluctuations at that time were at a level of 10^{-5}. Meantime, the modern space distribution of galaxies shows that the density contrast of inhomogeneities has changed dramatically: the initial perturbation growth due to gravitational instability resulted in the formation of gravitationally bound structures — dark matter halos. The inhomogeneity scale in these halos increased with time. The mean scale on which the present-day matter distribution in the Universe becomes linear, i.e., proportional to the radius cube, is about 10 Mpc. However, this scale can be larger or smaller in different regions of the Universe, depending on the mass of matter in the specific region (see, e.g., monograph [1] and recent reviews [2–5]).

It follows that the CMB temperature anisotropy map is the most important probe to study the Universe. However, from the standpoint of understanding the physical conditions at different evolutionary stages of the Universe, the CMB spectrum is equally important. The CMB spectrum brings information about the thermal history of the Universe, i.e., about the state of matter in the past and its interaction with radiation. The CMB spectrum to a very high accuracy corresponds to the Planck distribution, thus suggesting that matter in the past was in thermodynamic equilibrium (TE). Any physical processes leading to deviations from TE or to energy injections would leave imprints in the CMB spectrum, and the characteristics of these spectral features could be uniquely connected with the redshift z at which the energy was injected and with the energy injection mechanism.

A detailed theory of the interaction of matter with radiation in the early Universe was first developed in papers by Zeldovich, Kurt, and Sunyaev [6–8] and by Peebles [9] (see also monograph [10]). In these papers, CMB spectral distortions due to radiation processes during the primeval plasma recombination were first investigated, CMB spectral deviations from the equilibrium due to Compton scattering on hot electrons were calculated in detail, and CMB spectral distortions due to energy injection at different epochs were studied. All these topics are considered in this review in more detail, with special attention to be given to CMB spectral distortions during plasma recombination. We note that with the increasing accuracy of the CMB temperature anisotropy and spectrum measurements, these issues became very topical, and many papers by different authors have appeared in which the recombination theory was further elaborated and various types of CMB spectral distortions were studied. But the main ideas formulated in [6–9] remained unchanged (see Section 4).

Presently, all physical processes that occurred during the primeval plasma recombination epoch have been described in great detail and reproduced with high accuracy with many numerical codes (see Section 4.4). These numerical codes can be used for both the CMB anisotropy interpretation and the prediction of the amplitude and form of CMB spectral distortions when planning future experiments. In the first case, the accuracy of numerical calculations of the plasma recombination kinetics, including taking many subtle effects into account, is dictated by the high precision of CMB anisotropy measurements. For example, for successful interpretation of the Planck data, the dependence of the matter ionization degree on time should be calculated with an accuracy of up to 0.01%. In the second case, we are dealing with the extremely small amplitude of the CMB spectral distortions (otherwise, they would have already been discovered); the relative change in the CMB intensity due to these distortions, according to theoretical calculations, is less than 10^{-8}. Thus, here the accuracy of theory is much higher than the present-day experimental capacities. Therefore, the future discovery of the cosmological recombination spectrum (i.e., the collection of photons emitted during the primeval plasma recombination) seems to be very exciting. This, first, would be direct confirmation of the recombination stage in the early Universe, and, second, would provide an independent means to measure the baryon density in the Universe and other cosmological parameters.

At present, we completely understand all physical processes in the considered epoch and their observational manifestations. Now the matter depends on experiment. The experimental potential is currently increasing, and there is hope that the theoretical predictions will be confirmed by observations in the nearest future (see Section 5.3).

1.2 Before and after recombination: a brief history of the Universe

The period of recombination of the primeval hydrogen–helium plasma is one of the key evolutionary stages of the Universe and corresponds to the redshift interval $900 \lesssim z \lesssim 7000$. Due to expansion of the Universe, the temperature of matter decreased, plasma recombined, and radiation detached from matter, i.e., photons did not interact with matter (baryons) any more and traveled freely after recombination, only undergoing a redshift. Photons reach the observer at the redshift $z = 0$, and we observe them as the CMB. During recombination, the usual matter (baryons) passed from the ionized state to a neutral one, and the so-called period of neutral hydrogen (and helium) began. It is in

[1] *Wilkinson Microwave Anisotropy Probe*, the spacecraft launched by NASA to measure the CMB temperature anisotropy, operated in orbit from 2001 to 2010.

[2] The spacecraft of the European Space Agency to measure the CMB anisotropy with high precision, operated in orbit from 2009 to 2013.

[3] Sloan Digital Sky Survey (http://www.sdss.org).

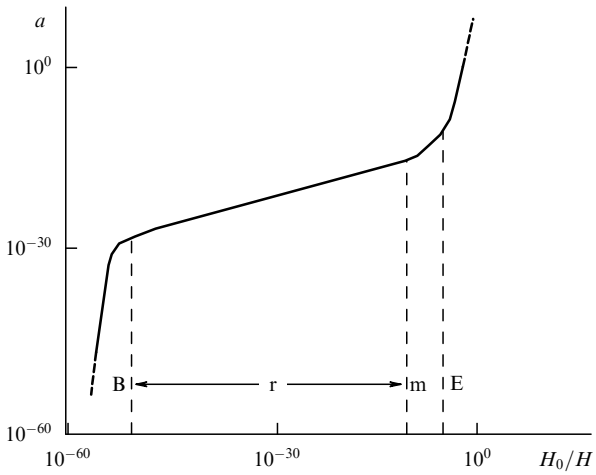

Figure 1. The scale factor of the Universe a as a function of the normalized Hubble radius H_0/H. Here, $H_0 = 67.3$ km s^{-1} Mpc^{-1} is the present-day Hubble constant. Marked are the Big Bang (B), radiation-dominated epoch (r), matter-dominated epoch (m), and dark-energy-dominated epoch (E). The boundaries between the epochs correspond to the time 10^{-36} s (B), 380,000 yrs (r), 10 bln yrs (m) from the beginning of expansion. (From [1].)

this period that small density perturbations grew to form gravitationally bound objects. With the recombination stage, the radiation-dominated epoch ended, and the nonbaryonic dark-matter-dominated stage began, during which dark matter particles formed gravitationally bound structures — halos — and cooled-down baryons settled toward the halo centers to form galactic disks. In Fig. 1, this time corresponds to the transition from the period marked with r to the period marked with m. We discuss this figure in more detail.

As is well known, matter in the Universe includes several components, differently contributing to the total density; according to the last data from the *Planck* experiment [11], these include dark energy ($\Omega_\Lambda/\Omega_0 \sim 68.3\%$), dark (nonbaryonic) matter ($\Omega_\mathrm{m}/\Omega_0 \sim 26.8\%$), regular (baryonic) matter ($\Omega_\mathrm{b}/\Omega_0 \sim 4.9\%$), massive neutrinos ($\Omega_\mathrm{v}/\Omega_0 \sim 0.1\%$), and radiation ($\Omega_\mathrm{r}/\Omega_0 \sim 0.01\%$). Here, $\Omega_i = \rho_i/\rho_\mathrm{cr}$ is the ratio of the density of the ith component to the critical density. The sum of all constituents Ω_0, which is equal to unity with high accuracy, determines the geometrical properties of the Universe and its evolution. According to the standard cosmological model, the Universe is expanding, and at large scales we observe the so-called Hubble flow, i.e., the recession of matter. The dynamics of this recession can be described in terms of the scale factor $a(t)$ dependence on the normalized Hubble radius H_0/H, where $H_0 = 67.3$ km s^{-1} Mpc^{-1} is the present-day Hubble constant [11]. This dependence is shown in Fig. 1. The power-law slope of this function, $\gamma^{-1} \equiv -(\mathrm{d}\ln a)/(\mathrm{d}\ln H)$, is larger than unity at the inflationary stage (B) and dark-energy-dominated stage (E), and is less than unity at the radiation- (r) and matter-dominated (m) stages. As can be seen from Fig. 1, during the radiation- and matter-dominated stages, the Universe expanded by 30 orders of magnitude. At the same time, the observed size of the Universe is about 10^{28} cm, which exceeds the Planck radius $l_\mathrm{Pl} \sim 10^{-33}$ cm by more than 60 orders of magnitude! Therefore, the size of the modern Universe cannot be explained without assuming the inflationary (exponential) stage of expansion.

Presently, the idea of an inflationary expansion of the Universe at the very early stages is commonly recognized [12]. The idea of inflation, which was first proposed by Gliner [13, 14] (see also [15, 16]), was supported and developed by Starobinsky [17, 18] and later by Linde [19, 20] and Guth [21]. The concept of inflation states that the equation of state of matter in the very early Universe can be expressed as $p = -\rho$. Such a state, which is characterized by a negative pressure[4] (antigravity), leads to accelerated expansion of the Universe, when the scale factor increases exponentially with time: $a(t) \sim \exp(Ht)$, where $H(t) = \dot{a}/a$ is the Hubble constant. At the inflationary stage, H remains constant, but after the end of inflation, H starts changing with time; further expansion follows the Friedmann law $a(t) \sim t^\alpha$, where $\alpha < 1$, and the so-called Hubble flow is formed. Thus, the primary reason for the Hubble flow is antigravity, the inflationary recession of matter [22–25].

The inflationary model solves two principal conundrums of classical Friedmann cosmology. The first is the causality problem, which follows from the observed homogeneity and isotropy of the large-scale matter distribution and CMB properties. The physical size of a causally connected region at the time of recombination corresponds to two angular degrees. Because the properties of the CMB are identical at all angular scales, including those larger than 2°, the question arises: Why do causally disconnected regions demonstrate identical properties? The second difficulty comes from the flatness of the Universe, i.e., from the fact that the total density in the Universe is very close to the critical value ($\Omega_0 = 1$), and the curvature is equal to zero at all stages, including the very early times. These two difficulties can easily be overcome by introducing an inflationary stage in the early Universe, which started 10^{-42} s after the Big Bang and lasted only 10^{-36} s. The inflation provides that the size of a casually connected region in the past greatly exceeds the size of the present-day horizon. Independently of the initial curvature of the world, the exponential expansion during inflation makes the Universe highly flat.

The state of matter with negative pressure is unstable, and such matter ultimately decays to form the usual gravitating matter. The matter particles are in thermal equilibrium, and the relativistic equation of state (radiation-dominated phase) holds: $p = \epsilon/3$, where ϵ is the energy density. At the same time, the so-called baryonic asymmetry of the Universe emerges, i.e., the prevalence of baryons over antibaryons. As a result, we live in the Universe without antimatter, with a very small baryon-to-photon number density ratio $n_\mathrm{b}/n_\gamma \sim 10^{-9}$. This stage is called the hot baryogenesis epoch. At this stage, the characteristic particle energies amount to $\sim 10^{16}$ GeV.

When the temperature of matter decreased to $\sim 10^{16}$ K (particle energies ~ 1 TeV), the electroweak phase transition occurred. As a result, the weak and electromagnetic interactions, which had been united before that time, were separated into electromagnetic interactions, with a photon being the gauge boson, and weak interactions, with $\mathrm{W}_\pm$- and Z_0-bosons being the gauge bosons. Later, at a temperature of 10^{12} K (particle energies ~ 100 MeV), quark confinement occurred, i.e., free quarks could no longer exist and formed protons and neutrons. One second after the Big Bang, after the formation of protons and neutrons, the primordial nucleosynthesis epoch began, which lasted up to about 200 s after the Big Bang. During this period, light nuclei were

[4] In general, $p = w\rho$, where the parameter w can be variable in time.

synthesized: helium ^{4}He (its fraction amounts to $Y_{\rm He} \approx 0.25-0.26$), a small amount of ^{3}He, deuterium, and lithium. Heavier nuclei were synthesized at much later times in stars. About 300 s after the Big Bang, the temperature in the Universe dropped below the limit for helium and other light nuclei formation in nuclear reactions, and the relative number density of nuclei did not change any more. The temperature in this epoch was $T \sim (1-5) \times 10^9$ K, corresponding to particle energies $\sim 100-500$ MeV. At the redshift $z \approx 7000$, when the temperature was $T \approx 2 \times 10^4$ K, recombination of the primeval plasma started, as discussed above. The epoch of neutral hydrogen (also known as the 'dark ages') ended at redshifts $z \sim 10-20$, with reionization of matter at the stage of a nonlinear evolution of gravitationally bound objects (galaxies, galaxy clusters, and superclusters).

2. CMB and its properties

2.1 Discovery of CMB

The expansion of the Universe had been the only experimental test in cosmology until the mid-1960s. The new era began in 1965 when A Penzias and R Wilson discovered the CMB. As discussed in Section 1, CMB photons are observed from the last scattering surface, when the Universe cooled to a temperature of 3000 K due to expansion, which led to recombination of plasma. The age of the Universe at the recombination stage was around 380,000 years, and since then photons have been propagating freely, virtually without interacting with matter. The very existence of the CMB directly supports the hot model of the Universe's evolution (the Big Bang theory), proposed by Gamow in 1946 [26] (see also [27]). The history of the prediction and discovery of the CMB, which includes many interesting facts, is intriguing by itself. It can be found, for example, in monograph [28]. Here, we briefly mention only the main events.

The CMB was discovered by Penzias and Wilson, collaborators in the American firm Bell Laboratories. In 1964, when measuring radio emission from the Galaxy with a horn reflector, Penzias and Wilson tuned the detector to the wavelength $\lambda = 7.3$ cm to check the noise level. They directed the horn to a dark (radio quiet) area of the Galaxy, but the measured signal turned out to be unexpectedly high. After numerous tests they found that the signal being measured did not depend on the direction and was not connected with ground-based sources. Penzias and Wilson published this result in the *Astrophysical Journal* [29]. At the same time, another group of researchers including R Dicke, P J Peebles, P Roll, and D Wilkinson deliberately prepared a similar experiment aimed at testing the Big Bang theory predictions. A theoretical paper by those authors was published in the same issue of the *Astrophysical Journal* [30]. Later, both groups conducted observations at the wavelength $\lambda = 3$ cm and confirmed the existence of the CMB. In 1978, Penzias and Wilson won the Nobel Prize for the discovery of the CMB.

We note that the first predictions of the existence of the CMB as a relic of the hot past of the Universe were made by Gamow. But Gamow concluded that the CMB radiation, which, according to his calculation, could not have a temperature higher than 5–6 K at the present time, could not be observed against the background emission from stars and galaxies. Later, it was noted in [31] that in the radio band, the CMB intensity must exceed all known background emissions.

Interestingly, indirect evidence of the CMB existence were known long before its discovery. For example, in 1941, Canadian astronomer E McKellar discovered that interstellar cyan (CN) molecules absorb stellar emission, being in the rotational state with the excitation temperature 2.3 K [32]. This fact was explained only after the discovery of the CMB. In the middle of the 1950s, Soviet radio astronomer T Shmaonov detected, using a horn, a background space radio emission at the wavelength 3.2 cm. He published this result [33], but because the measurement accuracy was not high, nobody paid due attention to this discovery at that time.

2.2 CMB anisotropy

The interaction of the CMB with matter prior to recombination and during recombination up to the last scattering surface leave traces both in the spatial distribution of the CMB (anisotropy) and in its energy spectrum (spectral distortions). The last scattering surface is a 'snapshot' of the Universe at the moment of the last scattering of photons on free electrons. The last scattering surface redshift corresponds to the time at which the optical depth for Thomson scattering attains unity, $\tau_{\rm rec}(z_{\rm r}) = 1$. The value of $z_{\rm r}$ can be obtained by approximating the results of numerical calculations of the recombination kinetics, i.e., from the dependence of the matter ionization degree on time (or redshift). For example, in [34], the following approximation was obtained:

$$z_{\rm r} \approx 1089 \left(\frac{\Omega_{\rm m} h^2}{0.14}\right)^{0.0105} \left(\frac{\Omega_{\rm b} h^2}{0.024}\right)^{-0.028} . \qquad (1)$$

The main imprints of interactions are caused by the Sachs–Wolf effect [35], the Silk effect [36], and Doppler scattering on moving electrons [37]. These effects determined the primary spatial anisotropy of the CMB imprinted on the last scattering surface immediately before the end of the recombination epoch. Later, secondary CMB anisotropy arose due to the Sachs–Wolf effect and gravitational lensing, and the smearing out of the primary anisotropy occurs due to the CMB photon scattering on moving electrons after reionization at $z \leqslant 10-30$ (see monograph [28] and review [38] for more details).

The CMB anisotropy was discovered by the COBE[5] experiment and the Relikt-1[6] experiment [40, 41]. The leaders of the COBE experiment, G Smooth and J Mather, won the Nobel Prize for this discovery in 2006. After the dipole anisotropy subtraction, the CMB temperature fluctuations are $\Delta T/T \sim 10^{-5}$. These fluctuations and acoustic peaks in the angular spectrum of the CMB anisotropy were predicted by Zeldovich and Sunyaev as early as 1970 [37], and were measured with high accuracy in numerous ground-based experiments [CBI (Cosmic Background Imager), ACBAR (Arcminute Cosmology Bolometer Array Receiver), VSA (Very Small Array)], balloon [BOOMERANG (Balloon Observations Of Millimetric Extragalactic Radiation And Geophysics), MAXIMA (Millimeter Anisotropy eXperiment Imaging Array), Archeops] and space experiments (*WMAP*, *Planck*). The angular power spectrum of CMB temperature fluctuations obtained by the *Planck* experiment is shown in Fig. 2.

[5] *Cosmic Background Explorer*, the NASA spacecraft devoted to CMB studies, operated in orbit from 1989 to 1992.

[6] The Soviet experiment for CMB studies. The Relikt-1 satellite operated in orbit from 1983 to 1984.

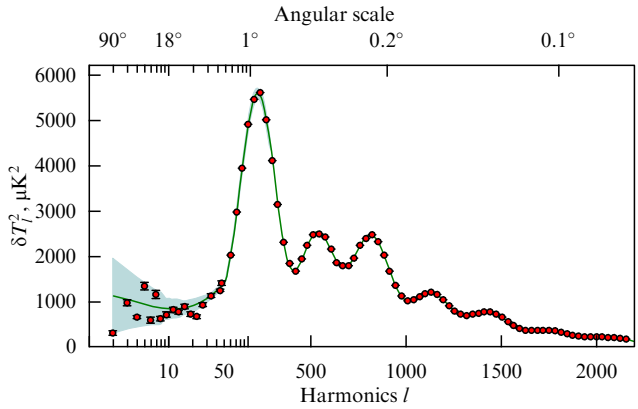

Figure 2. Angular power spectrum of the CMB temperature according to the *Planck* data [11]. The angular scale and the corresponding harmonic l are along the x axis, and the fluctuation amplitude squared on that scale, $\delta T_l^2 = l(l+1)C_l/(2\pi)$, is along the y axis.

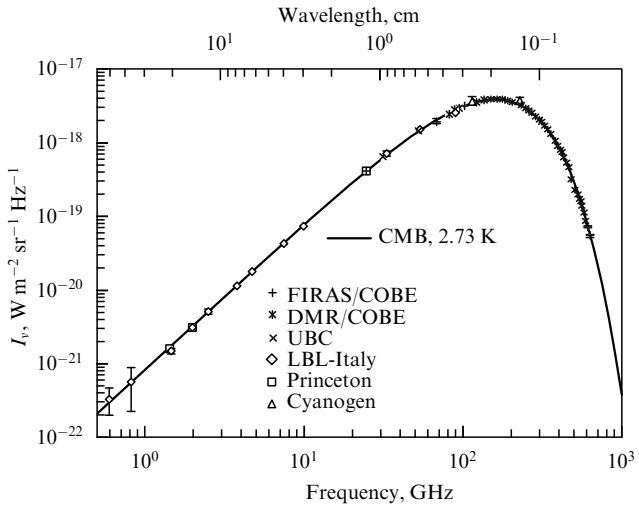

Figure 3. CMB spectrum from different experiments [43]. The radiation intensity I_ν is plotted versus the frequency and the corresponding wavelength.

2.3 Spectral characteristics of CMB

Since the discovery of the CMB in 1965, its temperature has been measured with increasing precision in various experiments over last several decades. The results of these experiments are listed, for example, in [28]. Here, we only note that by the beginning of the 1990s, more than 60 experiments had been carried out in the wavelength range from 1 mm to 73.5 cm. Most of these experiments were not accurate enough. The breakthrough occurred with the launch of the COBE satellite. According to COBE data, the CMB spectrum with an accuracy of 10^{-4} corresponds to a blackbody (Planck) radiation:

$$B_\nu = \frac{2h\nu^3}{c^2}\,\frac{1}{\exp\left(h\nu/k_{\rm B}T\right)-1}\,, \qquad (2)$$

where $k_{\rm B}$ is the Boltzmann constant, with the present-day temperature $T_0 = 2.725 \pm 0.001$ K [42]. These measurements were done by the FIRAS (Far Infrared Absolute Spectrometer) instrument aboard the COBE satellite in the wavelength range from 0.1 mm to 1 cm. Figure 3 shows the FIRAS/COBE blackbody spectrum of the CMB; measurements by other instruments are also shown for comparison.

The CMB fills space homogeneously, and its energy density exceeds that of any other background radiation (see Table 1). The CMB is the brightest sky emission from the meter to the submillimeter wavelengths. The present CMB photon number density is $n_{\rm ph} = 411$ cm^{-3}, corresponding to the energy density 0.25 eV cm^{-3}. The maximum of the Planck function with the temperature $T_0 = 2.725$ K peaks at the frequency $\nu_0 = 1.6 \times 10^{11}$ Hz. Due to isotropic expansion of the Universe, the CMB temperature decreases as $T(z) = T_0(1+z)$, where T_0 is the present-day CMB temperature and z is the redshift. The blackbody form of the CMB emission remains unchanged during the expansion, such that $T_1/(1+z_1) = T_2/(1+z_2)$, where T_1 and T_2 are the CMB temperatures at redshifts z_1 and z_2.

Table 1. Electromagnetic energy distribution of cosmic backgrounds [28].

Frequency range	Intensity, W m^{-2} sr^{-1}	Energy density fraction
Radio	1.2×10^{-12}	1.1×10^{-6}
CMB	9.96×10^{-7}	0.93
IR	$(4-5.2) \times 10^{-8}$	0.04–0.05
Optical	$(2-4) \times 10^{-8}$	0.02–0.04
X-ray	2.7×10^{-10}	2.5×10^{-4}
Gamma	3×10^{-11}	2.5×10^{-5}

3. Thermal history of the Universe before the primeval plasma recombination

3.1 Evolution of matter composition in the early Universe

Starting from the primordial nucleosynthesis at $z \sim 10^8 - 10^9$ and up to the end of the recombination epoch at $z \sim 10^3$, the change in matter composition was determined by the baryon-to-photon number density ratio $\eta_{{\rm b}\gamma} = n_{\rm b}/n_\gamma$, by the relation between different plasma processes, and by the Universe expansion rate. These parameters completely determined the dynamics of the synthesis of light nuclei, thermalization of the background radiation and plasma recombination kinetics, and the spectral features of the background radiation arising during these epochs.

The ratio $\eta_{{\rm b}\gamma}$ does not change as the Universe expands, excluding periods where annihilation of different sorts of particles occurred or some additional mechanism of energy release operated. Indeed, the photon number density in the blackbody radiation is $n_\gamma \propto T^3 \propto (1/a)^3 \propto (1+z)^3$, where T is the radiation temperature. On the other hand, the baryon number density is $n_{\rm b} \propto 1/a^3 \propto (1+z)^3$. Thus, $n_\gamma/n_{\rm b} = {\rm const}$ during the expansion. This ratio, up to a numerical factor, is essentially the radiation entropy per baryon $S_\gamma/n_{\rm b} = (4/3)aT^3/n_{\rm b}$, where $a = 7.57 \times 10^{-15}$ erg cm^{-3} K^{-4} is the radiation density constant. This specific entropy is conserved during adiabatic expansion. During annihilation periods of particle–antiparticle pairs, the entropy of pairs was converted into photons, but the photon spectrum preserved the equilibrium form.

Presently, the analysis of the CMB angular anisotropy spectrum yields $\eta_{{\rm b}\gamma} \sim 10^{-9}$, in excellent agreement with the estimate of $\eta_{{\rm b}\gamma}$ inferred from the Big Bang nucleosynthesis theory [44]. This means that the ratio $n_{\rm b}/n_\gamma$ did not change significantly at $z \lesssim 10^8$, and its conservation at late stages of the evolution of the Universe after recombination is due to the

conservation of the number of photons, which no longer interact with matter.

The smallness of the parameter $\eta_{b\gamma}$ determines the starting time of synthesis of primordial elements, because light nuclei can be formed only when the temperature drops below the binding energy of each nucleus. Otherwise, a huge number of photons, electrons, and positrons, which are in thermodynamic equilibrium, would effectively destroy newly formed nuclei. The nuclear statistical equilibrium is preserved until the rate of the corresponding nuclear reactions becomes smaller than the expansion rate of the Universe. At that time, the relative number density of nuclei becomes frozen and remains constant at later times.

After nucleon–antinucleon annihilation at temperatures of $10^{12}-10^{13}$ K, the primeval plasma mostly consists of electrons, positrons, photons (with $n_{e^-} \sim n_{e^+} \sim n_\gamma$), neutrinos, muons, and a small admixture of nucleons. The equilibrium between protons and neutrons is sustained due to weak interaction reactions:

$$\mathrm{p} + \mathrm{e}^- \longleftrightarrow \mathrm{n} + \nu\,, \quad \mathrm{p} + \bar{\nu} \longleftrightarrow \mathrm{n} + \mathrm{e}^+\,, \quad \mathrm{p} + \bar{\nu} + \mathrm{e}^- \longleftrightarrow \mathrm{n}\,.$$

Here, p is a proton, e^- is an electron, e^+ is a positron, ν is an electron neutrino, $\bar{\nu}$ is an antineutrino, and n is a neutron.

As the temperature decreases further, the fraction of protons increases because the equilibrium number density ratio of neutrons and protons is $N(\mathrm{n})/N(\mathrm{p}) = \exp\left(-\Delta M c^2/k_\mathrm{B} T\right)$, where ΔM is the mass difference between a neutron and a proton. Here, the efficiency of the weak interaction reactions decreases, and ultimately the neutron-to-proton number density ratio becomes frozen, according to different estimates, at the level $N(\mathrm{n})/N(\mathrm{p}) = 0.15-0.19$. Later, neutrons combine with protons to form deuterium nuclei, $\mathrm{n} + \mathrm{p} \to \mathrm{D} + \gamma$, and the energy and number density of photons are no longer high enough to destroy the deuterium nuclei. The accumulation of nuclei and further nuclear reactions occur to form ^{4}He nuclei with the ultimate fraction $Y_\mathrm{He} = 0.25-0.26$. A small number of ^{3}He, D, Li, and Be nuclei are also formed. About 300 s after the start of the expansion of the Universe, the temperature decreased such that nuclear reactions leading to helium and other light nuclei formation could not go on any more, and hence their relative number density did not change in further evolution. By that time, muons and electrons had annihilated, and the entropy of radiation had increased. The radiation spectrum remained the blackbody one. The temperature by that time was $T \sim (1-5) \times 10^9$ K. Electrons that survived annihilation played an important role in the CMB spectrum formation. The reader can find more details on physical processes in the early Universe, for example, in classical reviews and Zeldovich and Novikov's monograph [10].

3.2 Spectral distortions of CMB during energy release in the early Universe

Studying the CMB spectral features allows reconstructing the thermal history of the Universe, because the CMB spectrum is determined by the interaction of photons with matter at early evolutionary stages. The assumption that there were deviations from the blackbody spectrum, which could be due to powerful additional energy sources in the early Universe or strong deviations of the state of matter from thermodynamic equilibrium, was rejected by the COBE experiment [45]. The measurements showed that the CMB spectrum is described by the Planck function to an accuracy of about 10^{-4}, which suggests that total thermodynamic equilibrium held between photons and matter in the past. It was shown theoretically [10] that this equilibrium should have been held starting from the very early stages of the Universe up to the threshold temperature corresponding to the electron–positron pair creation $T_{\mathrm{e}^+\mathrm{e}^-} \sim 2 m_\mathrm{e} c^2/k_\mathrm{B} \approx 10^{10}$ K, corresponding to the redshift $z \sim 5 \times 10^9$.

Indeed, thermodynamic equilibrium must be established if $t_\mathrm{rel} \ll t_\mathrm{exp}$, where t_rel is the relaxation time of the particle energy distribution to the equilibrium and t_exp is the characteristic time of change of plasma parameters, which is of the order of the Universe expansion time. In the electron–positron plasma, the time t_rel is determined by the annihilation rate of particles, which turns out to exceed the expansion time by 17 orders of magnitude, i.e., $t_\mathrm{rel}/t_\mathrm{exp} \sim 10^{-17}$. Therefore, the plasma equilibrium is maintained due to the processes $\mathrm{e}^+ + \mathrm{e}^- \longleftrightarrow 2\gamma$.

In the Universe with a small ratio $\eta_{b\gamma}$, the main process thermalizing radiation is the double Compton scattering on electrons

$$\mathrm{e}^- + \gamma \longleftrightarrow \mathrm{e}^- + \gamma' + \gamma''\,.$$

The rate of this process becomes insufficiently high to maintain the equilibrium photon distribution at the redshift [46]

$$z_\mathrm{th} = 2.0 \times 10^6 \left(1 - \frac{Y_\mathrm{He}}{2}\right)^{-2/5} \left(\frac{\Omega_\mathrm{b} h^2}{0.02}\right)^{-2/5}\,, \tag{3}$$

where Y_He is the helium mass fraction. Therefore, up to the redshift $z \approx 2 \times 10^6$, possible CMB deviations from the Planck spectrum must have been smeared out by the double Compton scattering on free electrons that remained after annihilation. This process, as well as the creation and absorption of photons in free–free transitions, occurs with a high rate and effectively destroys any spectral distortions due to possible energy injection at $z \gtrsim 10^7$.

The highly blackbody form of the CMB spectrum constrains possible sources of energy injection in the early Universe at $z < 10^7$. Such sources could include decays of unstable particles, dissipation of acoustic waves, and accretion onto primordial black holes. The form of spectral deviations of the CMB due to energy injection at $10^5 \lesssim z \lesssim 10^7$ is determined by Compton scattering, which establishes full kinetic equilibrium between photons and electrons:

$$\mathrm{e}^- + \gamma' \longleftrightarrow \mathrm{e}^- + \gamma''\,.$$

This process turns out to be fast in comparison with expansion, because the hydrogen is fully ionized. As for the blackbody emission, the photon number density is determined by temperature only; with the injection of additional energy, the Compton scattering leads to the Bose–Einstein photon distribution with the chemical potential m [8]:

$$F_\nu = \frac{2h\nu^3}{c^2\left\{\exp\left[(h\nu + m)/k_\mathrm{B} T\right] - 1\right\}}\,, \tag{4}$$

where $m = -\mu k_\mathrm{B} T$ depends on the photon number density and temperature, and the dimensionless coefficient $\mu \geqslant 0$. The CMB deviations from the blackbody spectrum in this case are referred to as μ-distortions. Such a distortion is most

prominent in the Rayleigh–Jeans part of the spectrum: $I_\nu \propto \nu^3$ instead of $I_\nu \propto \nu^2$. We recall that in the Rayleigh–Jeans approximation at $h\nu \ll k_B T$, the blackbody intensity is $B_\nu \propto \nu^2 k_B T$. The COBE data analysis yielded the estimate $\mu < 9 \times 10^{-5}$ [47].

In the period $10^3 \lesssim z \lesssim 10^5$, the Compton scattering could not establish full kinetic equilibrium between radiation and electrons, and the spectrum formed by this scattering was characterized by the parameter [7]

$$y = \int \frac{k_B(T_e - T_\gamma)}{m_e c^2}\, d\tau_e\,, \tag{5}$$

where T_e, T_γ, and τ_e are the electron temperature, the radiation temperature, and the optical depth for Compton scattering, and m_e is the electron mass. During Comptonization, the low-frequency Rayleigh–Jeans photons acquire energy from electrons due to the second-order Doppler effect. Such spectral deviations are referred to as y-distortions. An analysis of the COBE data yielded the estimate $|y| < 1.5 \times 10^{-5}$ [47]. As a result of multiple scatterings, the Comptonization gradually leads to establishing a Bose–Einstein spectrum, i.e., to μ-distortions. However, starting from a certain redshift z_c, any energy injection would lead to y-distortions only, because the Bose–Einstein distribution cannot be reached. This transition occurs when the Compton scattering optical depth is equal to one, $\tau_c(z_c) = 1$ [44]:

$$z_c \approx 5.1 \times 10^4 \left(1 - \frac{Y_{He}}{2}\right)^{-1/2} \left(\frac{\Omega_b h^2}{0.02}\right)^{-1/2}. \tag{6}$$

The radiation-dominated era ended with the primeval plasma recombination, which spanned the redshift interval $900 \lesssim z \lesssim 7000$. During recombination, the primeval plasma emitted photons that distorted the CMB blackbody spectrum. The collection of these 'superequilibrium' photons is called the cosmological recombination spectrum. In Section 5, we discuss the mechanisms of these CMB spectral distortions in detail.

For completeness, we mention that the processes leading to CMB spectral distortions can also occur in the post-recombination epoch. For example, during matter reionization at $z \sim 20-50$, Compton scattering is no longer effective because the matter density is low. Therefore, photons emitted in free–free transitions cannot be thermalized and must distort the CMB spectrum [7, 48]. In addition, the thermal Sunyaev–Zeldovich effect occurs, i.e., Compton distortions of the CMB spectrum during scattering on the hot intergalactic gas in galaxy clusters with the temperature $T_e \sim 10^7$ K at $z \lesssim 10$. This effect, which appears on angular scales of about one arc minute, has been registered by several experiments [49].

4. Recombination of the primeval hydrogen–helium plasma

4.1 Plasma emission during recombination

As the Universe expanded, its temperature decreased, and the plasma started recombining. At $z \simeq 5000-7000$, the recombination of double-ionized helium occurred, HeIII → HeII; then, at $z \simeq 1500-3000$, single-ionized helium recombined, HeII → HeI; and finally, at $z \simeq 900-1600$, recombination of hydrogen occurred, HII → HI. By the end of the recombination epoch at $z \sim 1000$, the temperature of matter and radiation decreased to $T \sim 3000$ K, and matter 'decoupled' from radiation. This time is called the last scattering epoch, or the translucence epoch. At later times, the radiation freely travels in space, because matter becomes transparent to radiation. As noted in Section 1.2, photons reach the observer at $z = 0$ being redshifted only, and we observe exactly them as the CMB.

The photons produced in transitions in hydrogen and helium atoms in the recombination epoch partially survive up to the present time [50, 51] and therefore distort the CMB blackbody spectrum. These distortions have been calculated in many papers [52–63]. Measurements of the wavelength, intensity, and shape of the recombination lines provide information on the plasma temperature, baryonic matter density, redshift of the recombination epoch, and its duration. From the experimental standpoint, the main difficulty is that the recombination spectrum is very weak in comparison with the main thermal background. This is a direct consequence of the small ratio of the number of recombining atoms and the number of the equilibrium CMB photons, $\eta_{b\gamma} \sim 10^{-9}$. However, the experimental possibilities are now increasing, and this task is becoming topical. First, the discovery of recombination lines would provide additional proof of the recombination epoch in the early Universe. Second, this discovery would offer an independent way to estimate the baryonic density in the Universe, because the cosmological recombination spectrum of hydrogen and helium directly depends on this parameter.

In general, calculating the intensity and profiles of recombination lines requires solving a nonstationary system of differential equations for atomic level populations jointly with the radiation transfer equation for these lines. However, these equations contain two small dimensionless parameters, $n_{b\gamma}$ and t_{rel}/t_{rec}; the last is the ratio of the relaxation time of the population of levels (with the principal quantum number $n \geqslant 2$) to the characteristic time of recombination (changes in the ionization degree) [64]. The smallness of these parameters allows dividing the cosmological recombination spectrum calculation into three subtasks, which can be solved independently.

The first subtask is to calculate the recombination kinetics, i.e., the dependence of the ionization degree on time (redshift). The input parameters here include the Hubble constant (the expansion rate of the Universe), the baryonic matter density, and the radiation temperature. In the pioneering papers by Zeldovich et al. [6] and by Peebles [9], the main conclusion was that the Universe is almost completely opaque in the resonance lines and in the Lyman continuum of hydrogen, and that the accumulation of neutral atoms in the plasma occurs mainly due to the two-photon decay of the 2s level. Because the probability of this process is small, the population of the ground state of hydrogen is vastly different from the equilibrium value, which results in a delay of the recombination rate in comparison with the equilibrium Saha–Boltzmann rate. The recombination kinetics are considered in Sections 4.2–4.4 in more detail.

The second subtask is to calculate the production rate of photons that are additional to the equilibrium CMB. If the plasma and radiation were in full TE, such photons, of course, would not be produced. But because there is some deviation from equilibrium (see below), not all transitions between atomic levels are compensated, i.e., $R_{ij}N_i \neq R_{ji}N_j$, where R_{ij}

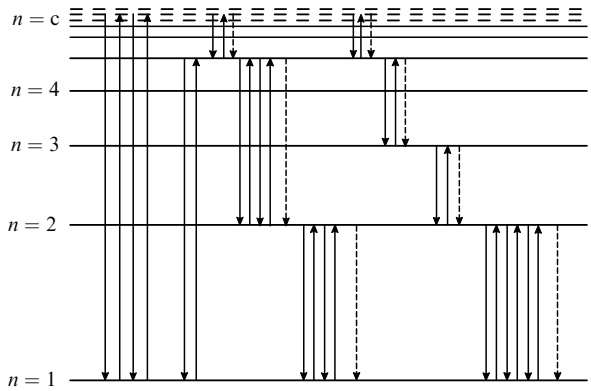

Figure 4. Hydrogen atom levels. The arrows show many possible transitions during the cosmological recombination epoch. Transitions that are eventually compensated are shown by solid arrows. The dashed arrows demonstrate that a small fraction of the transitions is not compensated by the reverse transitions due to a slight deviation of the atom number density in these states from equilibrium.

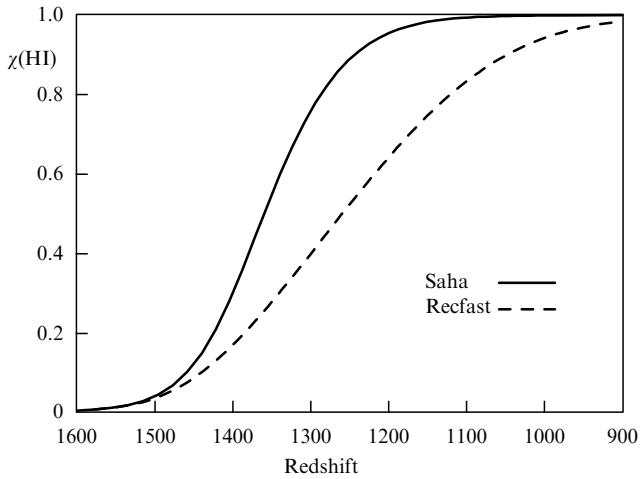

Figure 5. Delay of the hydrogen recombination compared to the equilibrium recombination. Shown is the fraction of neutral hydrogen atoms $\chi(\mathrm{HI})$ as a function of the redshift z calculated by the equilibrium Saha–Boltzmann formula (solid line) and using the Recfast code [66] (dashed line).

and R_{ji} are coefficients of radiative transitions between states i and j, and N_i and N_j are populations of the corresponding states. In TE with equilibrium populations N_i^0 and N_j^0, the detailed balance principle requires that $R_{ij}N_i^0 = R_{ji}N_j^0$. This is illustrated in Fig. 4, where levels of the hydrogen atom and transitions between them (arrows) are schematically shown. The dashed arrows demonstrate that a small fraction of the transitions between different states is not compensated by the reverse transitions due to small deviations of atomic number densities in these states from the equilibrium values. These deviations are due to expansion of the Universe, which is discussed in Section 4.2 in more detail. The collection of photons emitted in the uncompensated transitions forms the cosmological recombination spectrum, which we discuss in this review. We note that the concept of uncompensated transitions (or acts of irreversible recombination onto a certain level), first found in [52], does not reflect a specific physical process responsible for such transitions. This notion reflects the fact that physical conditions in the plasma and elementary processes in the considered epoch lead to incomplete compensation of transitions between levels and the emission of additional quanta. Moreover, this notion turns out to be convenient in calculations [54, 57, 64].

Radiation transfer in the recombination lines is the third part of the problem of calculating the CMB spectral distortions. The intensity of these distortions is very low, and therefore their effect on the recombination kinetics is insignificant. This enables simplifying the problem and, in fact, simply integrating over the entire recombination region, with the integrand given by a function that depends on values that were fully determined in the first two stages of the problem solution [54, 64].

We now discuss the stages described above in more detail. Historically, hydrogen recombination was studied first; recombination of helium was addressed somewhat later, and we follow this order for consistency.

4.2 Physics of recombination of the primeval hydrogen plasma

The hydrogen recombination epoch corresponds to the redshift interval $900 < z < 1600$, in which the temperature changed from 2200 to 4000 K. During this period, fully ionized hydrogen became neutral, with some residual density of electrons. We consider the main processes determining recombination. For a more detailed description of the processes occurring in the hydrogen plasma during recombination, the reader is referred to monographs [10, 28] and paper [65].

As was noted already in [6, 9], the primeval hydrogen recombination is 'delayed' compared to the equilibrium Saha–Boltzmann law:

$$\frac{n_\mathrm{e} n_\mathrm{p}}{n_\mathrm{HI}} = \frac{g_\mathrm{e} g_\mathrm{p}}{g_\mathrm{HI}} \frac{(2\pi m_\mathrm{e} k_\mathrm{B} T)^{3/2}}{h^3} \exp\left(-\frac{I}{k_\mathrm{B} T}\right), \tag{7}$$

where n_e, n_p, and n_HI are the number density of electrons, protons, and neutral hydrogen atoms, g_e, g_p, and g_HI are statistical weights, and I is the hydrogen ionization potential from the ground state. Figure 5 illustrates the ionization degree as a function of the redshift in two cases: calculated according to the equilibrium Saha–Boltzmann formula (7) and obtained in the numerical code Recfast [66] (see Section 4.4).

The delay occurs because the characteristic time to reach the equilibrium number density of hydrogen atoms is longer than the characteristic time of the plasma parameters changing (which is greater than the Universe expansion time by an order of magnitude). With a very high accuracy, the number density of neutrals can be taken to be equal to that of atoms in the ground state: $n_\mathrm{H} \approx n_1 = n_1^0 + \delta n_1$. Here, n_1^0 is the equilibrium population of the first level and δn_1 is the deviation of the first level population from the equilibrium value. The rate of change of n_1 with time is given by

$$\frac{\mathrm{d}n_1}{\mathrm{d}t} = \frac{\mathrm{d}n_1^0}{\mathrm{d}t} + \frac{\mathrm{d}(\delta n_1)}{\mathrm{d}t}\,. \tag{8}$$

In the case $\delta n_1 = 0$, we have the equilibrium recombination kinetics according to the Saha equation, because

$$\left.\frac{\mathrm{d}n_1}{\mathrm{d}t}\right|_{\delta n_1 = 0} = \frac{\mathrm{d}n_1^0}{\mathrm{d}t}\,. \tag{9}$$

The quantity $n_1^0/(\mathrm{d}n_1^0/\mathrm{d}t)$ is an order of magnitude greater than the Universe expansion time t_{exp} in the epoch considered. Now, if we mentally 'stop' the expansion, the rate of change in the atom number density in the ground state would be determined by the relaxation rate of the ground level to equilibrium,

$$\left.\frac{\mathrm{d}n_1}{\mathrm{d}t}\right|_{H(t)=0} = \frac{\mathrm{d}(\delta n_1)}{\mathrm{d}t}\,, \tag{10}$$

where $H(t)$ is the Hubble parameter characterizing the Universe expansion rate. Then the inequality

$$\left|\frac{\mathrm{d}n_1^0}{\mathrm{d}t}\right| \gtrsim \left|\frac{\mathrm{d}(\delta n_1)}{\mathrm{d}t}\right|_{H(t)=0} \tag{11}$$

would mean that the ground level population has no time to 'adjust' to the changing external conditions, and the equilibrium number density n_1^0 is not reached. As a result, the recombination is delayed, which is the case in our situation. We consider the hydrogen recombination mechanism in more detail to clarify why inequality (11) actually holds.

At redshifts $z \gtrsim 2000$, the matter and radiation temperature was $T \gtrsim 5500$ K, and the number densities of electrons, protons, and neutrals in the hydrogen plasma followed Saha equation (7). At that time, the number of ionizing quanta with the energy exceeding the ionization threshold $I_0 = 13.6$ eV was large, more than one quantum per baryon. Each act of recombination of an atom was balanced by ionization, and hence the equilibrium $\mathrm{p} + \mathrm{e} \leftrightarrow \mathrm{HI} + \gamma$ held, and neutral atoms hardly accumulated in the plasma. As the temperature decreased, the number of ionizing photons rapidly decreased, as can be easily seen from the formula for the number density of energetic quanta with $E \geqslant I_0$:

$$n_\gamma = \int_{I_0}^{\infty} \frac{8\pi\nu^2}{c^3}\,\frac{1}{\exp\left(h\nu/k_{\mathrm{B}}T\right) - 1}\,\mathrm{d}\nu\,. \tag{12}$$

In addition, at temperatures $T < 10^4$ K, the collisional ionization stops playing any significant role [65]. Thus, as the Universe expanded, the probability of ionization from the ground state decreased. It is important to note here that as long as the equilibrium number density of energetic quanta with $E \geqslant I_0$ decreases due to the general cooling of the Universe, the hydrogen recombination process starts, which produces such quanta (in recombination to the ground state). Hence, their number density must increase somewhat with respect to the equilibrium value. But because the absorption cross section of Lyman continuum photons $\mathrm{L_c}$ by neutral hydrogen is very high, the $\mathrm{L_c}$-photons emitted in direct recombination are immediately absorbed by neutral hydrogen atoms that are present in the plasma. Thus, the direct recombination to the ground state does not ultimately lead to the appearance of neutral atoms.

More probable is recombination through intermediate states according to one of the following channels:

1) $\mathrm{p} + \mathrm{e} \to \mathrm{H}_1^* + \gamma_{\mathrm{c}}\,,\quad \mathrm{H}_1^* \to \mathrm{H}_2^* \pm \gamma_l\,,\ \ldots,$
$\mathrm{H}_k^* \to \mathrm{H}_{2\mathrm{p}} + \gamma_l\,,\quad \mathrm{H}_{2\mathrm{p}} \to \mathrm{H}_{1\mathrm{s}} + \gamma_\alpha;$

2) $\mathrm{p} + \mathrm{e} \to \mathrm{H}_1^* + \gamma_{\mathrm{c}}\,,\quad \mathrm{H}_1^* \to \mathrm{H}_2^* \pm \gamma_l\,,\ \ldots,$
$\mathrm{H}_k^* \to \mathrm{H}_{2\mathrm{s}} + \gamma_l\,,\quad \mathrm{H}_{2\mathrm{s}} \to \mathrm{H}_{1\mathrm{s}} + 2\tilde{\gamma}\,.$

Here, $\mathrm{H}_{1,\ldots,k}^*$ denote hydrogen atoms in excited states, $\mathrm{H}_{1\mathrm{s}}$, $\mathrm{H}_{2\mathrm{s}}$, and $\mathrm{H}_{2\mathrm{p}}$ are atoms in 1s, 2s, and 2p states, γ_{c} is the $\mathrm{L_c}$-continuum photon, γ_l is the photon of the subordinate line, γ_α is the L_α-photon with the energy 10.2 eV, and $\tilde{\gamma}$ are two-photon continuum quanta produced by the 2s-level decays. We write '$\ldots \pm \gamma_l$' to indicate that the corresponding transition can occur in both emission and absorption.

For all excited states, nearly full ionization equilibrium $\mathrm{p} + \mathrm{e} \leftrightarrow \mathrm{H}^* + \gamma_{\mathrm{c}}$ is established, because there are enough photons with energies 3.4 eV or lower in the recombination epoch. We note that small deviations from equilibrium are present here due to the strong nonequilibrium of the ground state with which the excited states interact via radiative transitions.

As noted above, the absorption cross sections of Lyman-series photons and Lyman-continuum photons by neutral hydrogen are very high. Therefore, quanta with energies $E > E(\mathrm{L}_\alpha) = 10.2$ eV are absorbed by neutral atoms with the subsequent splitting into photons with lower energies down to L_α-photons. As a result, multiple emission and absorption of L_α-quanta occur, and their excess over the equilibrium background arises. It is this excess number density of L_α-quanta that leads to the cosmological hydrogen recombination delay. Ultimately, the irreversible hydrogen recombination occurs due to two processes: the two-photon transitions $2\mathrm{s} \to 1\mathrm{s}$ and the escape of L_α-photons from the line profile due to the Doppler diffusion and redshift in frequency in the expanding Universe. We briefly explain the essence of the second process.

The scattering of an L_α-photon occurs in two stages. First, an atom absorbs the photon in the line and then re-emits the photon in the same line. Due to thermal motion of the scattering atoms, the photon frequency after the scattering, measured in the comoving frame, differs from that before the scattering. The frequency change is on average about the Doppler width of the line. In addition, between scatterings, the photon frequency decreases due to redshift. The photon shift to the line red wing increases the photon mean free path and hence the photon energy redshift due to the cosmological expansion, and thus the photons ultimately stop interacting with neutral atoms.

We note that for resonance photons with energies $E > E(\mathrm{L}_\alpha)$, the escape from the corresponding line profile also occurs with the probability determined by the Sobolev probability p_{ij}, as for L_α-photons [see formula (13)]. But because the population of hydrogen levels with $n \geqslant 3$ is much smaller than that of the level with $n = 2$ ($N_3/N_2 \sim 10^{-3}$), the rate of this process, which is in fact proportional to the population of the corresponding level, turns out to be low, and hence the escape of resonance quanta other than the L_α-quanta can be neglected.

The Sobolev probability of the photon escape due to scatterings in a medium with a velocity gradient [67] (for example, in the expanding stellar envelopes) is a very good instrument to describe the photon escape from line profiles in the expanding Universe. Generally, this probability can be written as $p_{ij} = \exp\left(-\tau(\nu_{ij})\right)$, where $\tau(\nu_{ij})$ is the optical depth for the absorption of photons with the frequency ν_{ij} along the line of sight. The physical meaning of the probability p_{ij} is as follows: in the case $p_{ij} = 0$ (where $\tau(\nu_{ij}) \gg 1$), all corresponding photons are absorbed by atoms, and for $p_{ij} = 1$ (where $\tau(\nu_{ij}) \ll 1$) the photons are not absorbed and formally 'escape to infinity'. In [65], the Sobolev probability of escape was

expressed as

$$p_{ij} = \frac{1 - \exp(-\tau_S)}{\tau_S}\,, \tag{13}$$

where

$$\tau_S = \frac{A_{ji}\lambda_{ij}^3\left[N_i(g_j/g_i) - N_j\right]}{8\pi H(z)} \tag{14}$$

is the Sobolev optical depth for the absorption of photons with a wavelength λ_{ij} in the expanding Universe.

In the quasi-stationary approximation for diffusion of L_α-photons in the line wing (the characteristic diffusion time being much shorter than the characteristic recombination time), the probability for the photon to escape from multiple scatterings in the expanding Universe was calculated in [68] by solving the stationary transfer equation in the L_α line. The escape rate of L_α-photons was obtained in the form [68]

$$R_p = \frac{8\pi H}{\lambda_\alpha^3}\left[\frac{N_{2p}}{3N_1} - \exp\left(-\frac{h\nu_\alpha}{k_B T}\right)\right]\ \mathrm{cm}^{-3}\ \mathrm{s}^{-1}\,, \tag{15}$$

where N_i is the ith-level population, λ_α and ν_α are the wavelength and frequency of L_α-photons, T is the temperature, and H is the Hubble constant. Clearly, in the full thermodynamic equilibrium, $R_p = 0$ because the populations of all hydrogen levels are related by the Boltzmann law:

$$\frac{N_i}{N_{1s}} = \frac{g_i}{g_{1s}}\exp\left(-\frac{h\nu_{i1}}{k_B T}\right). \tag{16}$$

But due to expansion of the Universe, the equilibrium is violated, and the ground-state population turns out to be much lower than the equilibrium value, $N_{1s} \ll N_{1s}^0$. As regards populations of excited states, they are very close to equilibrium with the continuum, i.e., the equality $R_{ic}N_i = \alpha_i^c n_e n^+$ holds with good accuracy; the left-hand side of this equation is the photoionization rate from the ith level and the right-hand side denotes the recombination rate. However, small deviations from equilibrium do exist. For this reason, the CMB recombination spectrum appears.

We now consider two-photon transitions $2s \to 1s$. The 2s level of the hydrogen atom is metastable because single-photon transitions between states 2s and 1s are prohibited by the selection rules for dipole transitions. As a result of the $2s \to 1s$ transition, two photons are emitted, with the total energy being exactly equal to the transition energy. The rate of this process is $8.227\ \mathrm{s}^{-1}$. The inverse transition $1s \to 2s$ (two-photon absorption) also occurs, although its rate is much lower than the $2s \to 1s$ transition rate. This is because the ground-state population is much lower than the equilibrium value, $N_{1s} \ll N_{1s}^0$, and hence $A_{1s\to 2s}N_{1s} \ll A_{2s\to 1s}N_{2s}$. Clearly, these rates are equal in full thermodynamic equilibrium: $A_{1s\to 2s}N_{1s}^0 = A_{2s\to 1s}N_{2s}^0$.

In the hydrogen atom, two-photon decays are possible not only for the 2s level but also for higher levels. Probabilities of such transitions are estimated in [69], with the conclusion that they are important for calculations of helium recombination kinetics [70]. Later, it was shown in [71] that the two-photon decays of levels with $n > 2$ do not strongly affect the hydrogen recombination kinetics; their contribution to the hydrogen recombination rate is several percent [71] (see also Section 4.4).

We can conclude that the main processes leading to an increase in the number density of hydrogen atoms in the ground state are the L_α-quanta from the line profile in $2p \leftrightarrow 1s$ transitions and two-photon decays of the 2s state: $2s \to 1s$. The rates of these processes are small compared with the rate of change of the equilibrium plasma ionization degree, and therefore they cannot provide the equilibrium population of the ground state of hydrogen atoms, and recombination is delayed relative to the prediction of the equilibrium Saha equation.

4.3 Basic methods of primeval plasma recombination kinetics calculations

Numerical methods of recombination kinetics calculations can be conventionally divided into two types. The first essentially amounts to solving differential equations describing the evolution of the distribution function of atoms over energy states during recombination in an expanding Universe. In different papers, different numbers of levels were considered, and different assumptions were made as to how the kinetics of the higher levels, which do not explicitly appear in the equations, should be taken into account. For example, in papers by Zeldovich et al. [6] and Peebles [9], only the second level of the hydrogen atom was explicitly written in the equations, and upper states were taken into account by approximating the full recombination coefficient on all levels. In complete calculations [65], the system of differential equations for 300 hydrogen-atom levels was solved for populations of each level, coupled with differential equations for the matter temperature and radiation intensity. In the numerical code Recfast [66, 72], the kinetics are calculated using a three-level atom model (1st, 2nd level + continuum), and the effect of higher excited states is taken into account by introducing the recombination coefficient that is approximated differently than in other papers.

The second group of methods is based on the use of the so-called quasi-steady approximation [52]. The essence of this approximation is that instead of solving the system of differential equations, one solves the system of population balance equations for discrete levels with the principal quantum number $n \geqslant 2$. Indeed, the relaxation of the distribution of excited atoms occurs on the characteristic timescale of the order of the time of allowed transitions between the excited levels, $t_{rel} \sim 10^{-8}$ s. On the other hand, the characteristic time of change in the rate of processes that link the considered ensemble of atoms to the ground state of the atom and continuum is of the order of the characteristic time of expansion of the Universe in that epoch, $t_{exp} \sim 10^5$ years. Therefore, the ratio t_{rel}/t_{exp} is so small that the level distribution of atoms with $n \geqslant 2$ can be considered stationary. Then, for each level $n = i$, we can write the population balance equation and solve the system of such equations at each time step during the recombination epoch [64]:

$$\sum_{j=1}^{K} R_{ji}N_j - L_iN_i + B_i = 0\,, \tag{17}$$

where N_i is the ith-level population, the term $R_{ji}N_j$ describes transitions inside the ensemble of atoms with $n \geqslant 2$, L_iN_i takes processes leading to the escape from the ensemble into account (photionization, transition to states that are not explicitly present in the system of equations), B_i describes the processes leading to the appearance of new

atoms in the ensemble, and K is the number of equations in the system.

In such a setup, the ground-state population of the hydrogen atom is determined by the small rate of 'sinking' of atoms from the second level to the first level due to two-photon transitions 2s $\rightarrow$ 1s and the escape of L_α-quanta from the line profile. This sinking is responsible for the non-equilibrium distribution of atoms over excited states.

The use of the quasi-steady approximation significantly simplifies the numerical problem. This approximation was first used in [52] in calculations of the intensity of subordinate hydrogen lines produced during recombination. In paper [68] mentioned in Section 4.2, this approximation was also apparently used, because the statistical equilibrium equations for levels with $n \geqslant 2$ were solved there.

4.4 Recombination of the primeval helium plasma and modern methods of recombination kinetics calculations

During the period when the temperature of matter in the Universe was higher than 10^5 K, the matter constituted a proton–electron plasma with some number of helium nuclei immersed in a radiation field of very high intensity. The maximum of the photon energy distribution in this period corresponds to an energy much exceeding the helium ionization potential $I_{\rm He} \approx 54.4$ eV and the hydrogen ionization potential from the ground state $I_{\rm H} \approx 13.6$ eV. Hence, until a certain time, there could be no neutral atoms in the plasma, because a huge number of ionizing photons would immediately destroy them. However, with decreasing the temperature, the plasma started gradually recombining, and first of all a recombination of helium into HeII and then HeI occurred. The helium recombination epoch spanned the redshift range $z = 7000-1500$, and the temperature of matter at that time changed from 20,000 K to 4000 K.

Unlike initial calculations, for example, in [73], which were carried out using a three-level model of the HeI atom, modern numerical calculations are performed using multi-level HeI and HeII models (which include up to several hundred levels), with account for the fine structure. This allows both singlet and triplet energy states to be correctly taken into account. The results of numerical calculations show that the HeIII $\rightarrow$ HeII recombination occurs, in fact, according to the Saha–Boltzmann law

$$\frac{(\chi_{\rm e} - 1 - f_{\rm He})\chi_{\rm e}}{1 + 2f_{\rm He} - \chi_{\rm e}} = \frac{(2\pi m_{\rm e} k_{\rm B} T)^{3/2}}{h^3 n_{\rm H}} \exp\left(-\frac{I_{\rm HeII}}{k_{\rm B} T}\right), \qquad (18)$$

where $\chi_{\rm e} = n_{\rm e}/n_{\rm H}$ is the matter ionization degree, $f_{\rm He} = n_{\rm He}/n_{\rm H}$ is the helium-to-hydrogen number density ratio, $I_{\rm HeII}$ is the HeII ionization potential, and $n_{\rm H}$ is the total hydrogen number density. The same result for the HeII kinetics was also obtained in earlier papers. It was argued in [65] that from the standpoint of formation of HeII ions, direct recombination into the ground state is ineffective because the photons resulting from such a free–bound transition would be immediately absorbed by HeII ions that were already present in the plasma. The same is true for other resonance photons: their optical depth for absorption is very high. More effective recombination occurs via intermediate states, including the $n = 2$ level. Ultimately, the two-photon decay of the 2s level, whose rate is $\Lambda^{\rm HeII}_{2{\rm s}\rightarrow 1{\rm s}} = 526.5$ s^{-1}, is the main mechanism responsible for recombination. The rate of this process, $N_{2{\rm s}}\,\Lambda^{\rm HeII}_{2{\rm s}\rightarrow 1{\rm s}}$, where $N_{2{\rm s}}$ is the 2s-level population, determines the HeIII $\rightarrow$ HeII recombination rate. Because this rate is higher than the recombination rate of electrons into the $n = 2$ level, electrons do not stay in this state for long and rapidly transit into the ground state.

Thus, the recombination HeIII $\rightarrow$ HeII occurs in the equilibrium regime and ends at the redshift $z \approx 5000$. As regards HeI, modern numerical calculations give significantly different results from those in the first papers on recombination kinetics. First, the HeI recombination occurs in a regime that is strongly different from the equilibrium one described by the Saha–Boltzmann equation. The HeI recombination is delayed until the beginning of the hydrogen recombination at $z \approx 1500$. We note that in the first papers devoted to this problem, helium became fully neutral long before the hydrogen recombination began.

Originally, in [65], two-photon decays $2^1{\rm S}_0 \rightarrow 1^1{\rm S}_0$, whose rate is $\Lambda^{\rm HeI}_{2^1{\rm S}\rightarrow 1^1{\rm S}} = 51.3$ s^{-1}, and the transitions $2^1{\rm P}_1 \leftrightarrow 1^1{\rm S}_0$ were thought to be the main recombination mechanisms determining the recombination rate HeII $\rightarrow$ HeI. The effective recombination rate due to these processes in both cases is small compared to the rates of other radiative processes (transitions between excited states, as well as between excited states and the continuum). As a result, recombination proceeds more slowly than the equilibrium Saha equation for HeI predicts. That the helium recombination epoch ends very close to the hydrogen recombination epoch is explained by the similar mechanism leading to the formation of neutral HeI and H atoms, as well as by the fact that the ionization energies of these atoms from the $n = 2$ state are of the same order. Later, the HeI recombination was revised in [70] with two-photon decays of high levels of parahelium and transitions in the intercombination line of orthohelium $2^3{\rm P}_1 \leftrightarrow 1^1{\rm S}_0$ (one-photon transition between the triplet and bottom singlet states with the rate 177.58 s^{-1}) taken into account. This significantly increased the HeI recombination rate with respect to calculations in [65], and according to the calculations in [70], the 50% degree of ionization of the helium plasma is reached at about $z \approx 2200$ (for comparison, the same value in [65] is reached at $z \approx 1800$). However, the authors of [70] overestimated the contribution from two-photon decays, and, as was later shown in [74], this process does not significantly contribute to the helium recombination rate. Nevertheless, correctly taking the triplet helium transitions into account noticeably brings the HeI recombination kinetics closer to the equilibrium ones, although the recombination delay relative to adiabatic Saha recombination persists. According to [75], the ionization degree of the whole hydrogen–helium plasma, and not only of the helium component, changes by slightly more than 1% at $z \approx 1800$ due to taking $2^3{\rm P}_1 \leftrightarrow 1^1{\rm S}_0$ transitions into account.

Later, numerical calculations in [66], which were realized in the Recfast numerical code, were modified in [72], taking absorption of the resonance HeI quanta by neutral hydrogen into account, which accelerated the HeII $\rightarrow$ HeI recombination. Due to this process, the helium recombination ends at $z \approx 1800$, i.e., significantly earlier than found in [66]. The same effect was considered in [77], where an analytic solution was found to take the partial frequency redistribution of resonance quanta into account when describing the neutral hydrogen effect on the kinetics of HeII $\rightarrow$ HeI recombination. The above effects change the ionization degree of the primeval hydrogen–helium plasma by up to 2–3%, which is especially important for interpreting the CMB anisotropy data using the Recfast code. As regards the ionization degree

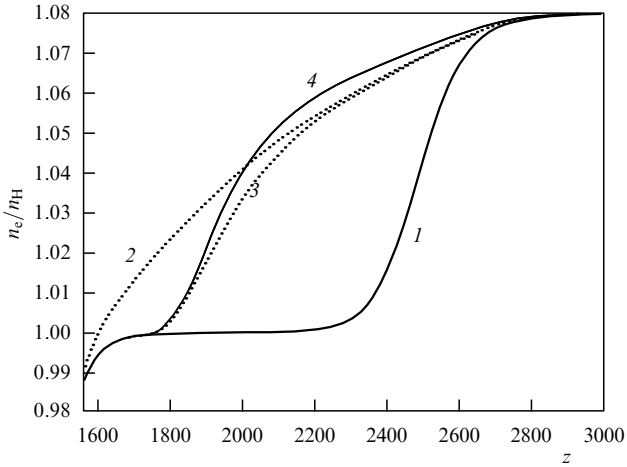

Figure 6. Kinetics of helium HeI recombination according to [78]. Shown is the plasma ionization degree as a function of the redshift n_e/n_H. Curve *1* corresponds to the equilibrium recombination HeI according to the Saha formula. Curve *2* shows the HeI recombination calculated by the Recfast code [66]. Curve *3* is obtained with neutral hydrogen effects taken into account. Curve *4* is obtained with both neutral hydrogen and back absorption of resonance quanta taken into account.

of the purely helium component, taking neutral hydrogen into account radically changes the helium recombination kinetics: at $z \approx 1900$, the degree of ionization of helium HeI decreases by 100% [78]. We note that to a certain degree, the helium recombination rate is also dependent on the effect of the inverse absorption by neutral helium and hydrogen atoms of the resonance quanta escaped from the wing of the corresponding resonance line due to the redshift: this process somewhat delays recombination at the initial stage.

To summarize, we reproduce Fig. 6 from [78], showing the plasma ionization degrees during the HeII $\rightarrow$ HeI recombination calculated taking the discussed processes into account, ignoring them in the Recfast code, and according to the equilibrium Saha equation.

By the present time, several groups have elaborated numerical methods for calculating the ionization degree of the primeval helium–hydrogen plasma as a function of the redshift. These include Recfast [66, 72], RICO [79], RecSparse [80], HyRec [81], CosmoRec [82, 83], Atlant [84], and SPDCBR [85–87]. These numerical codes are based on a certain physical model of recombination. This model includes a system of kinetic equations describing the change in populations of excited atomic states and the plasma ionization degree with time, the radiation transfer equation in lines, and some fine effects that eventually affect the recombination rate and the cosmological recombination spectrum at the 1% level. The difference between the models used in different numerical codes can lie in the number of levels explicitly accounted for in calculations, in the analytic approximations used for the recombination coefficient to upper levels lying close to the continuum, and in the number of effects that affect both the radiation transfer in different lines and populations of levels.

The launch of the WMAP and Planck missions made a leap forward in CMB anisotropy observations and the accuracy of measurements. This demanded an increased precision of the theoretical predictions that are used to interpret observational data. In particular, to successfully analyze the Planck data, the accuracy of numerical calculations of the plasma ionization degree must be at least 0.1% for the hydrogen recombination epoch and 1% for the helium recombination epoch; it would be better if this accuracy were an order of magnitude higher [84]. This fact initiated a large number of papers where the recombination theory is improved by taking various fine effects into account. We briefly discuss some of them.

The correction to the rate of two-quantum transitions 2s $\leftrightarrow$ 1s due to the induced transition effects is discussed in [88, 89]. In [89], the effect of L_α-emission generated by hydrogen recombination on these transitions was correctly taken into account. In general, according to the estimates in [89], this improvement changes the ionization degree by 0.5% to delay the recombination at $z \lesssim 1200$. The recoil during scattering in the L_α line, which accelerates the hydrogen recombination, was taken into account in [90], and the correction to the ionization degree at $z = 900$ was found to be 1.3%. The effect of collisional transitions 2s $\leftrightarrow$ 2p on the 2s and 2p level populations was studied in [91], with the conclusion that in the cosmological recombination epoch, these transitions do not establish the equilibrium distribution over sublevels of the $n = 2$ level, and their effect can be neglected. Some papers considered two-photon transitions from upper levels of the hydrogen atom [70, 71, 75]. It was shown that two-photon cascade transitions could correct the plasma ionization degree by fractions of a percent. Later, these transitions were considered in detail in paper [92], which studied the behavior of line wings that can play a significant role in the deviation of the recombination rate from the standard value. The back absorption by neutral hydrogen and helium atoms of resonance photons that escaped the wing of the corresponding resonance line due to the redshift was also investigated in [93, 94]. The inclusion of this effect into the recombination kinetics changes the respective ionization degree of hydrogen and helium by ~ 0.2 and ~ 0.12 percent.

We now turn to the discussion of the CMB spectral distortions (the cosmological recombination spectrum) arising due to plasma emission during recombination.

5. CMB spectral distortions during recombination of the primeval plasma

5.1 Short-wavelength CMB spectral distortions

It is convenient to consider the short-wavelength and long-wavelength CMB spectral distortions separately. This is not due to some principal difference in the spectral distortion formation mechanisms, but mostly due to different detection techniques in future observations. At short wavelengths ($\lambda \lesssim 300$ μm), observations will be significantly hampered by the presence of a high cosmic infrared background formed by emissions from distant galaxies (Fig. 7). At the same time, there is no such strong background in the centimeter and decimeter bands, which facilitates the detection. In addition, Earth's atmosphere is transparent in these bands and observations can be carried out by ground-based facilities. The relative distortions of the CMB intensity in these bands can be up to 10^{-5} [51]. It is also important that the CMB intensity is stronger at centimeter wavelengths than at short wavelengths with $\lambda \lesssim 200$ μm by several orders of magnitude.

The appearance of CMB spectral distortions in the Wien part was first studied by Zeldovich et al. [6] and Peebles [9]. It was recognized in these papers that the specifics of hydrogen recombination in the early Universe causes the modern CMB spectrum at $\lambda \lesssim 200$ μm to be distorted due to the

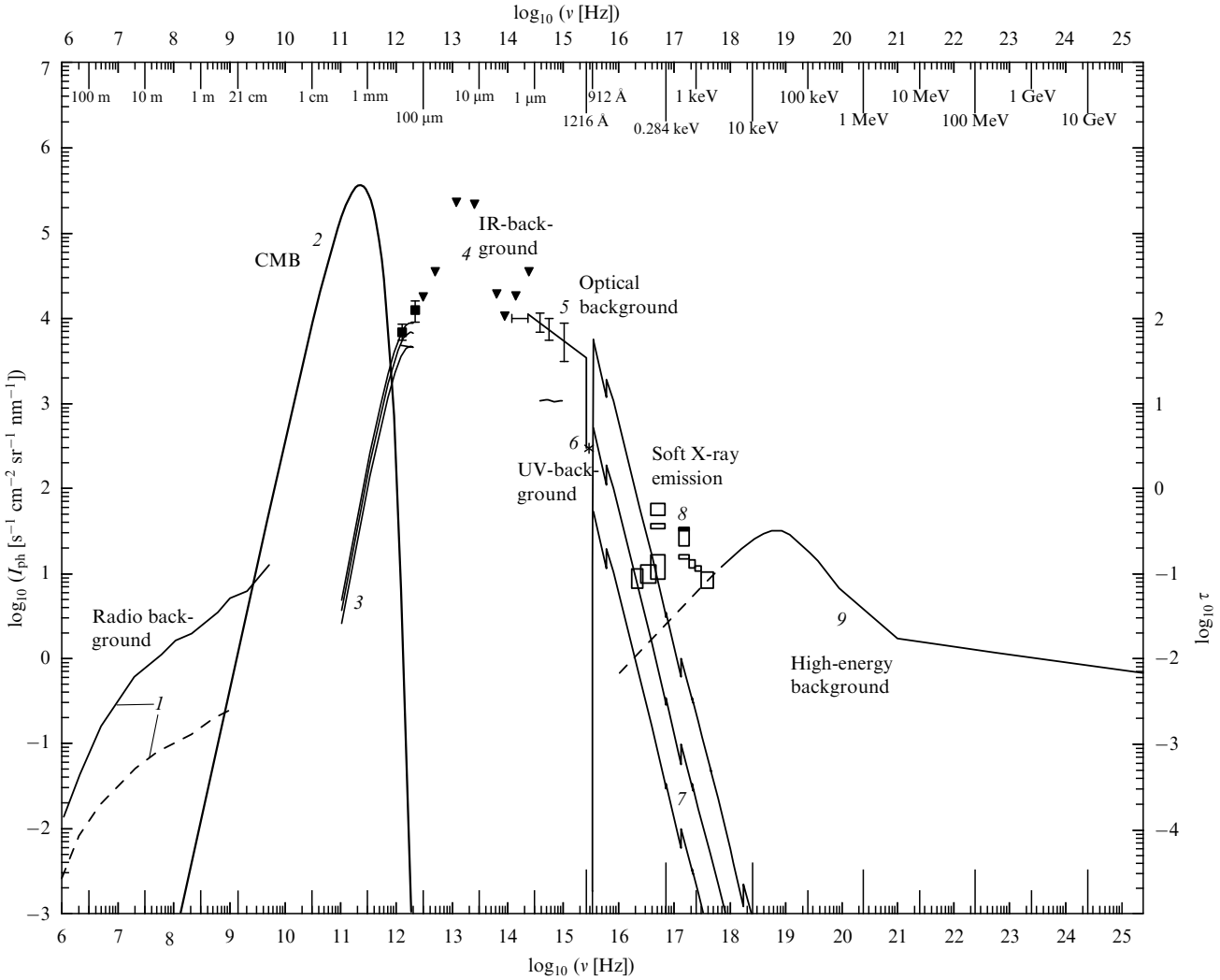

Figure 7. Cosmic background radiation spectrum of the Universe. $I_{\rm ph}$ is the photon flux intensity, ν is the frequency, τ is the optical depth. *1* — radio background from the galactic pole (dashed curve) and galactic plane (solid curve); *2* — CMB spectrum measured by FIRAS/COBE; *3* — spectrum of extragalactic microwave background radiation excess relative to the blackbody spectrum with the temperature 2.72 K (according to FIRAS/COBE data); *4* — infrared background at 140 and 240 μm (dark squares) and upper limits at higher frequencies (dark triangles); *5* — optical background: measurements (dots with error bars); the solid line passing through the dots is the low-frequency extrapolation of the UV background; the short, nearly horizontal line below these dots is the integral brightness of galaxies in the deep Hubble survey; *6* — UV background; the asterisk is the upper limit according to the *Voyager* spacecraft measurements; the solid vertical line is the model L_α-spectrum from ionized intergalactic clouds at high redshifts; *7* — optical depth for absorption of hard UV radiation by the interstellar medium for hydrogen column densities 10^{19}, 10^{18}, and 10^{17} cm^{-2} (from right to left); *8* — soft X-ray emission: rectangles (the width is unimportant, the height corresponds to different measurement intervals); *9* — high-energy background: the dashed straight line is a low-frequency extrapolation. (According to the data in [95].)

two-photon emission and L_α-emission. At $\lambda \lesssim 200$ μm, the CMB intensity should be several orders of magnitude higher than the Planck spectrum intensity. For example, in the flat cosmological model framework ($\Omega = 1$), the CMB intensity at $\lambda = 100$ μm was calculated to increase from $\sim 10^{-26}$ erg (cm^2 s Hz sr)$^{-1}$ [9] to $\sim 10^{-24}$ erg (cm^2 s Hz sr)$^{-1}$ [6], while the Planck spectrum intensity at this wavelength is $B_\nu \approx 4 \times 10^{-33}$ erg (cm^2 s Hz sr)$^{-1}$. The general impression on the shape of these distortions can be obtained from inspection of Fig. 8 taken from [53].

Indeed, as a result of multiple acts of absorption and emission, as well as of cosmological redshift in the expanding Universe, L_α-photons shift toward lower frequencies and eventually move out from the line wing. Hence, these photons cannot excite any more neutral hydrogen atoms from the ground state to the $n = 2$ level, and the 'escape' of L_α-quanta becomes one of the hydrogen recombination mechanisms. Of course, frequency-shifted ('reddened') L_α-photons can be absorbed by hydrogen atoms in excited states, but the probability of this process is vanishingly small because the number of atoms in excited states is many orders of magnitude smaller than the number of atoms in the ground state ($n_2/n_1 \sim 10^{-14}$ in the recombination epoch). Hence, the optical depth for absorption of L_α-photons by neutral atoms is very small, and these photons become 'excess' relative to the equilibrium radiation background. Because the L_α wavelength is $\lambda_0 \approx 0.12$ μm and the maximum escape rate of L_α-quanta from the profile wing occurs at the redshift $z \approx 1400$ [65], the L_α-line peak presently has the wavelength $\lambda = \lambda_0 \times 1400 = 170$ μm.

CMB spectral distortions due to L_α-emission have been calculated by many authors since 1968. For example, in [68], radiation transfer in the L_α-line was considered taking partial frequency redistribution and recoil during scatterings into

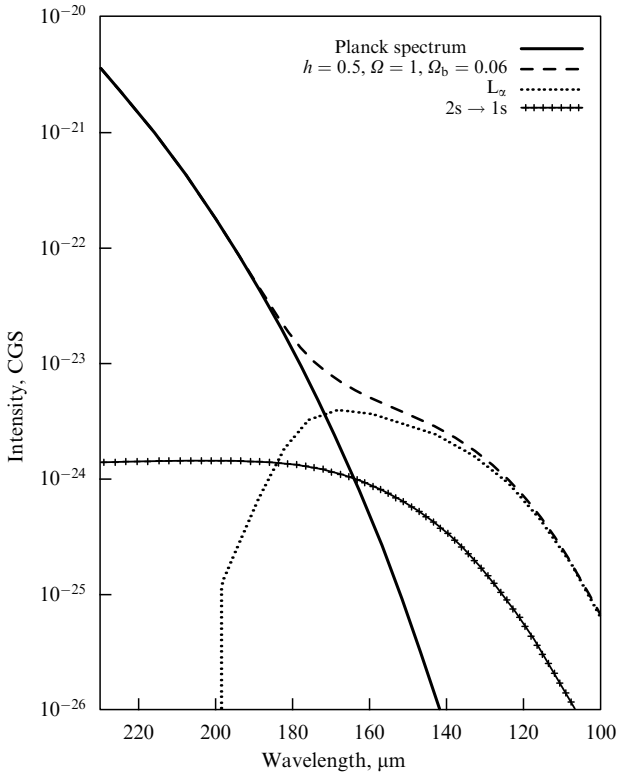

Figure 8. CMB distortions due to the excess L_α-quanta emission and two-photon transitions according to [53]. Cosmological parameters are shown in the figure, $h = H_0/100$ km s^{-1} Mpc^{-1}, where H_0 is the modern Hubble parameter value.

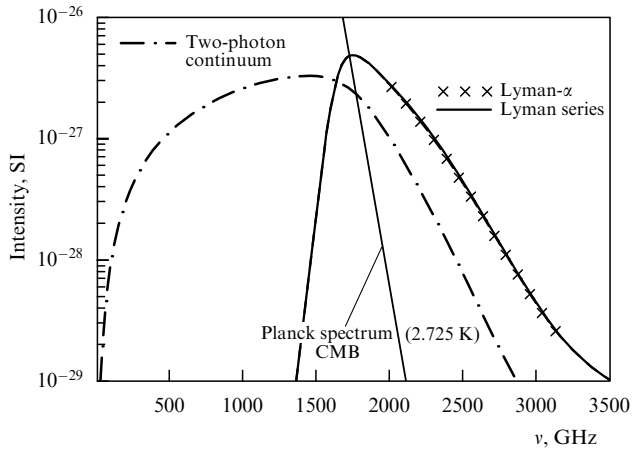

Figure 9. CMB distortions due to the excess Lyman-series quanta (solid curve) and two-photon emission according to [58]. The L_α-line (the curve marked with crosses that almost coincides with the solid curve) contributes most to the Lyman distortions; its peak intensity is 4.8×10^{-27} W m^{-2} sr^{-1} Hz^{-1}. Calculations for the standard cosmological models with the parameters $\Omega_b = 0.044$, $\Omega_m = 0.268$, $\Omega_\Lambda = 0.732$, and $h = 0.71$.

account. As a result, the L_α-line intensity at $\lambda = 100$ μm was calculated to be $I_\nu \sim 10^{-26} - 5 \times 10^{-25}$ erg (cm^2 s Hz sr)$^{-1}$ [68]. In [53], the CMB spectral distortions due to L_α-emission and two-photon emission in the $2s \to 1s$ transition were calculated. The results are presented in Fig. 8, which demonstrates the contribution of distortions due to L_α-emission and two-photon transitions and the total distortions of the CMB spectrum for cosmological parameters $\Omega = 1$, $\Omega_b = 0.06$, and $H_0 = 50$ km s^{-1} Mpc^{-1}.

Later, several groups reconsidered this problem using more precise calculations of the recombination kinetics [58, 59]. The results of calculations of the L_α- and 2γ-distortions obtained in [58] are shown in Fig. 9. The two-photon spectrum has a much broader profile than the L_α-line profile, and therefore these distortions lie in virtually one spectral band, i.e., they overlap.

Thus, in most papers, the CMB intensity changes due to the L_α-photon excess and two-photon continuum amount to 10^{-24} erg (cm^2 s Hz sr)$^{-1}$, and the CMB intensity increases by about a factor of two. However, such a substantial intensity increase does not facilitate the detection of these recombination distortions, because the background emission from different cosmic sources falls within the corresponding wavelength range. The Cosmic Infrared Background (CIB) intensity exceeds that of the CMB together with its distortions at $\lambda \lesssim 200$ μm. However, the CMB spectral distortions have a specific shape, which can be used to distinguish them from the smooth CIB. But in any case, the problem of decomposition of the total signal into separate components, including the distorted CMB, is very difficult, and can be solved only with increasing experimental capabilities in the future.

5.2 Emission during transitions between higher levels of hydrogen and helium atoms

We now consider plasma emission during transitions between higher levels of hydrogen atoms with $n \geqslant 2$. The emission of atoms in subordinate lines during recombination was first considered in [50], but the first numerical calculations of CMB distortions caused by this emission were performed later [54, 57, 58].

As shown above, the dynamic equilibrium between excited atomic states and the continuum is constantly maintained due to a large number of transitions $p + e \leftrightarrows H^* + \gamma_c$ and $H_i \leftrightarrows H_j + \gamma_c$. Here, H^* and $H_{i,j}$ denote the hydrogen atom in some excited state and in the states with $n = i, j$, and γ_c is a continuum-spectrum photon. As a result, populations of excited levels are found in a state that is very close to equilibrium with the continuum. However, due to expansion of the Universe, certain deviations of level populations from equilibrium arise, because not all $i \leftrightarrow j$ transitions are eventually balanced. A small fraction of the total number of transitions turns out to be uncompensated, which results in the emission of excess photons (relative to the equilibrium background), and is essentially why the recombination occurs. This picture is illustrated in Fig. 4. The dashed arrows show one of the possible cascades due to which the atom eventually turns out to be in the ground state, i.e., an 'irreversible' act of recombination occurs. Photons emitted during such a cascade are uncompensated and become excess relative to the blackbody CMB spectrum.

To characterize the efficiency of the excess photon production in the line $i \to j$, it is convenient to use the quantity first introduced in [52] — the efficiency coefficient of the corresponding transition $\eta_{ij} = Z_{ij}/Z_{12}$, where Z_{ij} and Z_{12} are the rate of uncompensated transitions from level i to level j (which is usually expressed in the units cm^{-3} s^{-1}), and from the second to the ground level. This coefficient has a clear physical meaning: η_{ij} is the mean number of photons emitted in the transition $i \to j$ per act of uncompensated recombination into the ground state. The transition efficiency was calculated in great detail in [64], where deviations of the populations of excited states from equilibrium were also

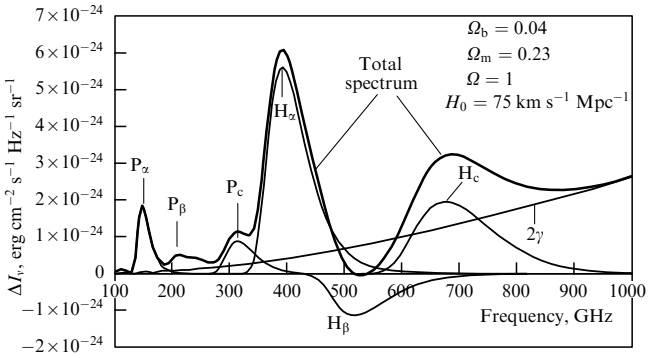

Figure 10. Balmer H_α and H_β lines and the Paschen P_α line in the cosmological recombination spectrum. Parameters of the ΛCDM model used are shown in the figure.

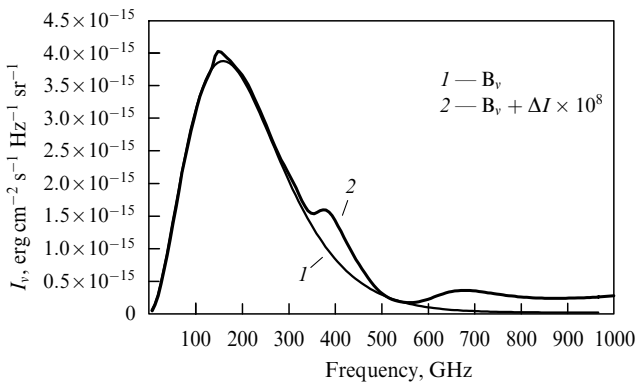

Figure 11. Cosmological hydrogen recombination spectrum (intensity enhanced by a factor of 10^8) superimposed on the CMB blackbody spectrum. ΔI is the Planck intensity B_ν change due to CMB recombination distortions. The ΛCDM model with the parameters $H_0 = 75$ km s^{-1} Mpc^{-1}, $\Omega_b = 0.04$, and $\Omega_m = 0.23$ is used.

obtained and the numbers of uncompensated line transitions were calculated. Numerical calculations were included by Burgin in the code SPDCBR [85–87], which was used in [54] to calculate the intensity of H_α and P_α recombination lines. The results of the calculations are presented in Figs 10 and 11. All calculations were done for the flat cosmological ΛCDM model with the parameters $\Omega_\Lambda = 0.7$, $\Omega_b = 0.04$, and $H_0 = 75$ km s^{-1} Mpc^{-1}. Figure 10 shows lines H_α, H_β, P_α, continua H_c and P_c, and the wing of the two-photon continuum 2γ. The H_α line is the strongest and has a peak intensity of 6×10^{-24} erg cm^{-2} s^{-1} Hz^{-1} sr^{-1}. Figure 11 demonstrates distortions, which are enhanced by a factor of 10^8 for clarity and are superimposed on the blackbody CMB spectrum.

Using the physical model in [64], the authors of [57] independently calculated the efficiency of different transitions and obtained results coincident up to 1%. For the Rayleigh–Jeans CMB spectral distortions (at $h\nu_{ij} \ll k_B T$), the authors of [57] calculated the relative CMB temperature change as

$$\frac{\Delta T}{T} = \frac{c^3}{8\pi\nu_{ij}^3}(1+z)\,\frac{\mathrm{d}x_p}{\mathrm{d}z}\,\frac{h\nu_{ij}}{k_B T(z)}\,N_{tot}(z)\eta_{ij}\,, \qquad (19)$$

where x_p is the fraction of free protons in the plasma and $N_{tot}(z)$ is the full number density of hydrogen. The relative CMB distortions in the frequency range 1–100 GHz are then $\Delta T/T \lesssim 3 \times 10^{-7}$. The ratio $\Delta T/T$ decreases as the frequency increases and reaches 10^{-10} at 100 GHz; the distortions themselves are fairly low-contrast. We note that the drop in relative CMB distortions is due to the CMB intensity itself decreasing by more than three orders of magnitude in the frequency range under consideration.

Interestingly, with the fine structure of the hydrogen atom taken into account, the efficiency coefficient η_{ij} becomes negative for some lines. This means that during hydrogen recombination, photons with certain frequencies are more likely to be absorbed than emitted; hence, 'absorption' features should arise in the cosmological recombination spectrum. In other words, at certain frequencies, the CMB intensity is slightly lower than the equilibrium value, while the brightness of the background is enhanced at other frequencies due to excess photons. We consider this process in more detail.

We assume that channels of the 'irreversible' recombination into the ground state due to uncompensated line transitions 2s ↔ 1s and 2p ↔ 1s are 'switched off'. Then, clearly, complete equilibrium between all excited hydrogen levels, plasma, and radiation is established. In this case, due to the principle of detailed balance, all cascade transitions are compensated, because any pair of transitions between levels $i \leftrightarrow j$ is compensated. Let now irreversible recombination channels from the second level to the ground level be 'turned on'. These channels cause nonequilibrium, because cascades leading to the ground state (which are uncompensated) appear among many possible cascades. Photons emitted in such cascades are also uncompensated, and hence there is an excess relative to the equilibrium background.

We consider the situation where an electron recombines to the 2p level of a hydrogen atom (directly or through intermediate levels). Then there are three further possibilities for the electron.

First, the electron can be photoionized in the continuum directly or through intermediate states. No neutral hydrogen atom is formed in this case, however, and in the end these cascades produce no excess photons, because all such cascades are mutually compensated on average (see above).

Second, the electron can transit into the ground state due to scatterings and L_α-photon escape from the line wing, which results in the appearance of a neutral hydrogen atom and excess photons.

Third, the electron can transit into the 2s state through several transitions via upper levels, and from this state, the electron can ultimately transit into the ground 1s state due to irreversible recombination via two-photon decay. Two (the simplest) possible trajectories allowed by the selection rules and realizing the third case are presented in Fig. 12. It is seen that in this cascade, one Balmer-series photon H_β is absorbed and one Paschen-series photon P_α and one Balmer-series photon H_α is emitted.

Thus, with the splitting of levels with respect to the orbital momentum l taken into account, uncompensated transitions to the ground state lead to both absorption and emission of photons with different frequencies.

The same conclusion was reached in [58] and [63], where the cosmological recombination spectrum was calculated taking the dependence of the hydrogen level populations on the orbital quantum number l into account. The CMB spectral distortions in the frequency range from 1 GHz to 3500 GHz were calculated. The splitting of states into angular momentum l substates was shown to significantly affect the

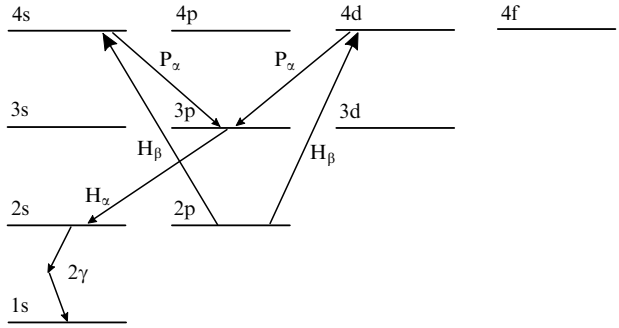

Figure 12. Scheme of one possible trajectory of electron transitions between hydrogen levels that results in absorption of a photon from the equilibrium background.

shape and intensity of the hydrogen recombination lines. The result is shown in Fig. 13 taken from [63]. Here, an important note should be made with regard to the helium recombination spectrum. In Section 4.4, we discussed the acceleration of HeI recombination due to the absorption of resonance helium quanta by residual neutral hydrogen atoms in plasma. This significantly affects the CMB distortions arising during helium recombination, because the acceleration of recombination enhances the contrast of helium recombination lines (the lines become more narrow). Additionally, photons absorbed by neutral hydrogen are later emitted in the L_α line to form a spectral feature near 1100 GHz [63]. Thus, in addition to the main recombination L_α line, a weaker L_α line arises in the spectrum emitted by hydrogen in the helium HeI recombination epoch (in Fig. 13, it can be seen to the right of the main L_α line).

To measure the cosmological recombination spectrum accurately enough to determine Ω_b, the measurement errors must be an order of magnitude smaller than for the recombination line intensity. This means that the measurements must be carried out at a level of $\Delta I \sim 10^{-25}$ erg cm^{-2} s^{-1} Hz^{-1} sr^{-1}.

5.3 Notes on possible future methods of observations

Because the CMB spectrum is identical in all directions, any area in the sky can be observed, preferably where the contribution from other cosmic backgrounds is minimal. It is also important that the sought signal must be unpolarized, which can be used to separate it from other sources. To search for CMB distortions, the spectrum should be scanned in a wide frequency range. It will not be necessary to measure the absolute value of the radiation intensity; it will be sufficient to search for deviations of the intensity from the blackbody value, i.e., the 'modulated' signal with an amplitude of 10–30 nK and $\Delta\nu/\nu \sim 0.1$. Some researchers now consider the 10 nK accuracy to be reachable by modern instrumentation.

Apparently, the best method would be to seek a maximum correlation between the observed and predicted spectra shown in Figs 10 and 13. In our opinion, a modulating Fourier spectrometer for the frequency range 100–1000 GHz (from 3 mm to 300 μm) with the spectral resolution $R = \lambda/\Delta\lambda \sim 10$ could be most promising for this purpose.

6. Conclusion

The prediction and further measurement of temperature fluctuations of the CMB have been the most important milestones both in research on the early Universe and in the development of measurement techniques. In the last 15 years, progress in experimental technologies has allowed the CMB measurement accuracy to increase by orders of magnitude. On the one hand, this has enabled different cosmological parameters to be determined with high precision (or to be constrained), which has greatly improved our understanding of the Universe. On the other hand, this progress has demanded more precise theoretical predictions for successful data analysis. In particular, in recent years, many papers have appeared that address the details of cosmological recombination of the primeval plasma — the most important stage in the evolution of the Universe, during which primordial hydrogen and helium became neutral and radiation separated from matter. In fact, we can study the CMB at the moment of last

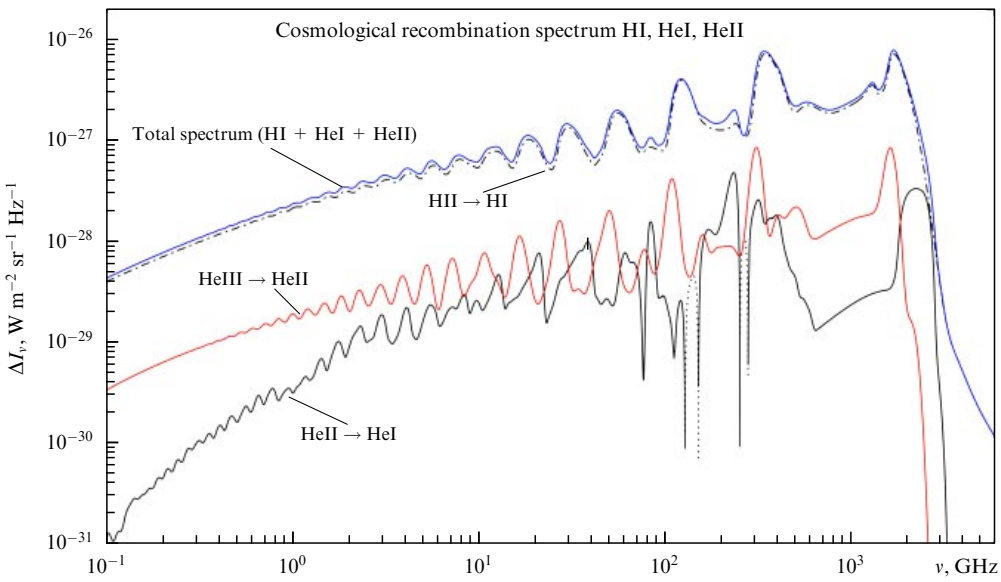

Figure 13. Cosmological recombination spectrum of hydrogen and helium in accordance with the calculations in [63]. Contributions from recombination spectra of hydrogen and helium into the total spectrum are shown separately. The dashed lines show absorption spectral features. The calculations are done for the standard cosmological model.

scattering of photons on electrons and infer information about that epoch from the CMB spatial and spectral features.

Presently, virtually all physical processes occurring in the recombination epoch at redshifts $900 < z < 7000$ have been well studied, and it can be asserted that the research of the last decade in this field reconstructs the complete picture of cosmological recombination and related effects. After the discovery of CMB temperature fluctuations, the challenging task is to measure unique CMB deviations from the Planck spectrum due to the photon emission during primeval plasma recombination. Measurements of these deviations will allow the improved determination of the CMB temperature (monopole component), of the baryon to photon ratio, of the primordial helium abundance, etc. It is also of fundamental importance that excess photons relative to the equilibrium CMB spectrum, which were emitted during recombination, are produced not near the last scattering surface when the CMB temperature anisotropy pattern is formed ($z_{\rm rec} \approx 1000$) but at earlier times. For example, the maximum density of photons emitted during hydrogen and helium (HeI and HeII) recombination occurs at respective redshifts $z \sim 1300-1400$, $z \sim 1800-1900$, and $z \sim 6000$, which allows 'looking behind' the last scattering surface.

The discovery of CMB recombination distortions would provide not only direct observational evidence of the primeval plasma recombination epoch but also a probe to study the thermal history of the Universe at that time. In particular, all physical processes (including both well-known and theoretically studied, and possible unexpected phenomena) that took place in that period affect the cosmological recombination spectrum in a certain way. Hence, precise measurements of this spectrum provide an invaluable probe for conditions and processes of cosmological recombination. Because the expected signal is extremely small (by the order of magnitude, $10^{-9}-10^{-8}$ times as small as the total CMB signal), its experimental discovery is very challenging. However, some researchers believe that such an unprecedentedly high accuracy of measurements can be realized in the near future. The recombination spectrum has features (mainly, the independence of the signal from the direction, the absence of polarization, and the characteristic wave-like shape of this spectrum) that could facilitate the detection of this weak signal.

7. Appendix. Comparison of primeval plasma recombination emission with nebular emission

From the methodological standpoint, it is interesting to compare the physical conditions in gas nebulae and in the primeval plasma in the recombination epoch, because the theory of nebular spectrum formation has much in common with the problem of the cosmological recombination spectrum generation. However, much more essential are differences that do not allow us to fully use the achievements of the theory of emission nebulae in the problem considered here.

As is well known, the glow of gas nebulae is caused by the emission of hot stars of early spectral types located in their centers. The nebula absorbs high-frequency stellar radiation and reprocesses it into low-frequency quanta. This suggests a strong deviation from thermodynamic equilibrium. Indeed, the radiation from the central star arrives at each point of the nebula strongly diluted, which is characterized by the dilution factor $W = \Omega/4\pi$, where Ω is the solid angle subtended by the star from a given point of the nebula. For the typical sizes of gas nebulae and their nuclei, the dilution factor is about 10^{-14}. Hence, the radiation density inside the nebula should be very small, $\rho_\nu = W\rho_\nu^*$, where ρ_ν^* is the radiation density of the star, assuming the blackbody emission. The spectrum of the radiation field in the nebula corresponds to a very high stellar temperature, and hence there is a huge mismatch between the radiation density and its spectrum. As a result, a photon frequency redistribution occurs: high-energy quanta turn into quanta with smaller wavelengths.

Thus, the main distinction of physical conditions in gas nebulae and in the cosmological plasma is that in the plasma we are dealing with an equilibrium radiation field with the temperature $T \approx 3500$ K, while in the nebulae the radiation field is highly nonequilibrium and has a low intensity, but its spectrum corresponds to the temperature $T \sim 20{,}000$ K.

Due to the low density, all neutral atoms in nebulae are in the ground state (we note that the plasma ionization degree there can be very high: the low radiation density is compensated by a relatively small number density of free electrons, $n_{\rm e} \approx 10^4$ cm^{-3}). Therefore, nebulae are opaque for the Lyman-series emission and are transparent in all subordinate series. Thus, the Balmer quanta and quanta from other subordinate series freely move out of the nebula. All cascade transitions downward in a hydrogen atom occur virtually without delay, because the number of soft photons is insufficient to ionize hydrogen from excited states. This means that the excited hydrogen states *are not* in equilibrium with the plasma or radiation.

A totally different situation occurs in the cosmological hydrogen plasma. In this case, in the Planck radiation field with the temperature about 3000–4000 K, there are many soft photons with the energies about 3.4 eV or less that are capable of maintaining the statistical equilibrium among the excited hydrogen atoms, plasma, and radiation.

If we compare the degree of nonequilibrium of matter in the nebulae and cosmological plasma, the ratio $n_{\rm e}n^+/n_1$ in the nebulae differs from the equilibrium Saha value by a factor of the order of the dilution coefficient $W \sim 10^{-14}$. At the same time, as shown in Section 4.2, the ionization degree of the cosmological plasma in the hydrogen recombination epoch cannot differ from the equilibrium Saha value by more than a factor of two. Taking these considerations into account, we can conclude that the theory of nebular spectra cannot be applied to the cosmological recombination spectrum. Nevertheless, these two theories largely share the same terminology because the recombination radiation mechanisms are similar in both cases.

References

1. Lukash V N, Mikheeva E V *Fizicheskaya Kosmologiya* (Physical Cosmology) (Moscow: Fizmatlit, 2010)
2. Lukash V N, Mikheeva E V, Malinovsky A M *Phys. Usp.* **54** 983 (2011); *Usp. Fiz. Nauk* **181** 1017 (2011)
3. Doroshkevich A G, Lukash V N, Mikheeva E V *Phys. Usp.* **55** 3 (2012); *Usp. Fiz. Nauk* **182** 3 (2012)
4. Gurbatov S N, Saichev A I, Shandarin S F *Phys. Usp.* **55** 223 (2012); *Usp. Fiz. Nauk* **182** 233 (2012)
5. Berezinsky V S, Dokuchaev V I, Eroshenko Yu N *Phys. Usp.* **57** 1 (2014); *Usp. Fiz. Nauk* **184** 3 (2014)
6. Zel'dovich Ya B, Kurt V G, Syunyaev R A *Sov. Phys. JETP* **28** 146 (1969); *Zh. Eksp. Teor. Fiz.* **55** 278 (1968)
7. Zeldovich Ya B, Sunyaev R A *Astrophys. Space Sci.* **4** 301 (1969); *Astrophys. Space Sci.* **4** 285 (1969)
8. Sunyaev R A, Zeldovich Ya B *Astrophys. Space Sci.* **7** 20 (1970)
9. Peebles P J E *Astrophys. J.* **153** 1 (1968)

10. Zel'dovich Ya B, Novikov I D *Stroenie i Evolyutsiya Vselennoi* (Structure and Evolution of the Universe) (Moscow: Nauka, 1975); *Sov. Phys. Usp.* **7** 763 (1965); *Usp. Fiz. Nauk* **84** 377 (1964); *Sov. Phys. Usp.* **8** 522 (1966); *Usp. Fiz. Nauk* **86** 447 (1965)
11. Ade P A R et al. (Planck Collab.), arXiv:1303.5076
12. Cherepashchuk A M *Phys. Usp.* **56** 509 (2013); *Usp. Fiz. Nauk* **183** 535 (2013)
13. Gliner E B *Sov. Phys. JETP* **22** 378 (1966); *Zh. Eksp. Teor. Fiz.* **49** 542 (1966)
14. Gliner É B *Sov. Phys. Dokl.* **15** 559 (1970); *Dokl. Akad. Nauk SSSR* **192** 771 (1970)
15. Gliner É B, Dymnikova I G *Sov. Astron. Lett.* **1** 93 (1975); *Pis'ma Astron. Zh.* **1** 7 (1975)
16. Gliner É B *Phys. Usp.* **45** 213 (2002); *Usp. Fiz. Nauk* **172** 221 (2002)
17. Starobinskii A A *JETP Lett.* **30** 682 (1979); *Pis'ma Zh. Eksp. Teor. Fiz.* **30** 719 (1979)
18. Starobinsky A A *Phys. Lett. B* **91** 99 (1980)
19. Linde A D *Phys. Lett. B* **108** 389 (1982)
20. Linde A *Particle Physics and Inflationary Cosmology* (Chur: Harwood Acad. Publ., 1990); Translated from Russian: *Fizika Elementarnykh Chastits i Inflyatsionnaya Kosmologiya* (Moscow: Nauka, 1990)
21. Guth A H *Phys. Rev. D* **23** 347 (1981)
22. Lukash V N, Mikheeva E V, Strokov V N *Phys. Usp.* **55** 204 (2012); *Usp. Fiz. Nauk* **182** 216 (2012)
23. Lukash V N, Mikheeva E V, Strokov V N *Phys. Usp.* **55** 831 (2012); *Usp. Fiz. Nauk* **182** 894 (2012)
24. Bolotin Yu L, Erokhin D A, Lemets O A *Phys. Usp.* **55** 876 (2012); *Usp. Fiz. Nauk* **182** 941 (2012)
25. Chernin A D *Phys. Usp.* **56** 704 (2013); *Usp. Fiz. Nauk* **183** 741 (2013)
26. Gamow G *Phys. Rev.* **70** 572 (1946)
27. Chernin A D *Phys. Usp.* **37** 813 (1994); *Usp. Fiz. Nauk* **164** 889 (1994)
28. Naselsky P D, Novikov D I, Novikov I D *Reliktovoe Izluchenie Vselennoi* (Cosmic Microwave Background in the Universe) (Moscow: Nauka, 2003)
29. Penzias A A, Wilson R W *Astrophys. J.* **142** 419 (1965)
30. Dicke R H et al. *Astrophys. J.* **142** 414 (1965)
31. Doroshkevich A G, Novikov I D *Sov. Phys. Dokl.* **9** 111 (1964); *Dokl. Akad. Nauk SSSR* **154** 809 (1964)
32. McKellar A *Publ. Dominion Observ. Ottawa* **7** 15 (1941)
33. Shmaonov T A *Prib. Tekh. Eksp.* (1) 83 (1957)
34. Hu W, in *Observing Dark Energy, Proc. of a Meeting, 18–20 March 2004, Tucson, Arizona, USA* (ASP Conf. Series, Vol. 339, Eds S C Wolff, T R Lauer) (San Francisco: Astronomical Society of the Pacific, 2005) p. 215; astro-ph/0407158
35. Sachs R K, Wolfe A M *Astrophys. J.* **147** 73 (1967)
36. Silk J *Astrophys. J.* **151** 459 (1968)
37. Sunyaev R A, Zeldovich Ya B *Astrophys. Space Sci.* **7** 3 (1970)
38. Hu W, Dodelson S *Annu. Rev. Astron. Astrophys.* **40** 171 (2002)
39. Smoot G F et al. *Astrophys. J. Lett.* **396** L1 (1992)
40. Strukov I A et al. *Sov. Astron. Lett.* **13** 65 (1987); *Pis'ma Astron. Zh.* **13** 163 (1987)
41. Strukov I A et al. *Mon. Not. R. Astron. Soc.* **258** 37P (1992)
42. Fixsen D J, Mather J C *Astrophys. J.* **581** 817 (2002)
43. Smoot G F, Scott D "Cosmic background radiation", http://www.astro.ubc.ca/people/scott/cbr_review.ps (2000); *Eur. Phys. J. C* **15** 145 (2000)
44. Hu W, arXiv:0802.3688
45. Mather J C et al. *Astrophys. J.* **420** 439 (1994)
46. Danese L, De Zotti G *Astron. Astrophys.* **107** 39 (1982)
47. Fixsen D J et al. *Astrophys. J.* **473** 576 (1996)
48. Zeldovich Ya B, Syunyaev R A *Sov. Astron. Lett.* **6** 285 (1980); *Pis'ma Astron. Zh.* **6** 545 (1980)
49. Carlstrom J E, Holder G P, Reese E D *Annu. Rev. Astron. Astrophys.* **40** 643 (2002)
50. Dubrovich V K *Sov. Astron. Lett.* **1** 196 (1975); *Pis'ma Astron. Zh.* **1** (10) 3 (1975)
51. Dubrovich V K, Stolyarov V A *Astron. Astrophys.* **302** 635 (1995)
52. Bernshtein I N, Bernshtein D N, Dubrovich V K *Sov. Astron.* **21** 409 (1977); *Astron. Zh.* **54** 727 (1977)
53. Boschan P, Biltzinger P *Astron. Astrophys.* **336** 1 (1998)
54. Dubrovich V K, Shakhvorostova N N *Astron. Lett.* **30** 509 (2004); *Pis'ma Astron. Zh.* **30** 563 (2004)
55. Dubrovich V K, Grachev S I *Astron. Lett.* **30** 657 (2004); *Pis'ma Astron. Zh.* **30** 723 (2004)
56. Rubiño-Martín J A, Hernández-Monteagudo C, Sunyaev R A *Astron. Astrophys.* **438** 461 (2005)
57. Kholupenko E E, Ivanchik A V, Varshalovich D A *Grav. Cosmology* **11** 161 (2005)
58. Rubiño-Martín J A, Chluba J, Sunyaev R A *Mon. Not. R. Astron. Soc.* **371** 1939 (2006); astro-ph/0607373
59. Wong W Y, Seager S, Scott D *Mon. Not. R. Astron. Soc.* **367** 1666 (2006)
60. Chluba J, Sunyaev R A *Astron. Astrophys.* **458** L29 (2006); astro-ph/0608120
61. Chluba J, Rubiño-Martín J A, Sunyaev R A *Mon. Not. R. Astron. Soc.* **374** 1310 (2007); astro-ph/0608242
62. Chluba J, Sunyaev R A *Astron. Astrophys.* **475** 109 (2007)
63. Rubiño-Martín J A, Chluba J, Sunyaev R A *Astron. Astrophys.* **485** 377 (2008)
64. Burgin M S *Astron. Rep.* **47** 709 (2003); *Astron. Zh.* **80** 771 (2003)
65. Seager S, Sasselov D D, Scott D *Astrophys. J. Suppl.* **128** 407 (2000)
66. Seager S, Sasselov D D, Scott D *Astrophys. J.* **523** L1 (1999)
67. Sobolev V V *Moving Envelopes of Stars* (Cambridge: Harvard Univ. Press, 1960); Translated from Russian: *Dvizhushchiesya Obolochki Zvezd* (Leningrad: Izd. Leningr. Gos. Ordena Lenina Univ., 1947)
68. Grachev S I, Dubrovich V K *Astrophysics* **34** 124 (1991); *Astrofiz.* **34** 249 (1991)
69. Dubrovich V K *Opt. Spectrosc.* **63** 256 (1987); *Opt. Spektrosk.* **63** 439 (1987)
70. Dubrovich V K, Grachev S I *Astron. Lett.* **31** 359 (2005); *Pis'ma Astron. Zh.* **31** 403 (2005)
71. Chluba J, Sunyaev R A *Astron. Astrophys.* **480** 629 (2008); arXiv:0705.3033
72. Wong W Y, Moss A, Scott D *Mon. Not. R. Astron. Soc.* **386** 1023 (2008)
73. Matsuda T, Satō H, Takeda H *Prog. Theor. Phys.* **42** 219 (1969)
74. Hirata C M, Switzer E R *Phys. Rev. D* **77** 083007 (2008)
75. Wong W Y, Scott D *Mon. Not. R. Astron. Soc.* **375** 1441 (2007)
76. Kholupenko E E, Ivanchik A V, Varshalovich D A *Mon. Not. R. Astron. Soc.* **378** L39 (2007); astro-ph/0703438
77. Kholupenko E E, Ivanchik A V, Varshalovich D A *Astron. Lett.* **34** 725 (2008); *Pis'ma Astron. Zh.* **34** 803 (2008)
78. Switzer E R, Hirata C M *Phys. Rev. D* **77** 083006 (2008)
79. Fendt W A et al. *Astrophys. J. Suppl.* **181** 627 (2009)
80. Grin D, Hirata C M *Phys. Rev. D* **81** 083005 (2010)
81. Ali-Haïmoud Y, Hirata C M *Phys. Rev. D* **83** 043513 (2011); arXiv:1011.3758
82. Chluba J, Thomas R M *Mon. Not. R. Astron. Soc.* **412** 748 (2011); arXiv:1010.3631
83. Chluba J, Thomas R M "CosmoRec: Cosmological Recombination code", Astrophysics Source Code Library record ascl:1304.017; http://asterisk.apod.com/wp/?page_id = 12
84. Kholupenko E E et al. *Mon. Not. R. Astron. Soc.* **417** 2417 (2011); arXiv:1104.3050
85. Burgin M S "SPDCBR library for calculation of cosmological recombination spectrum", ftp://ftp.asc.rssi.ru/outgoing/spdcbr/
86. Burgin M S *Bull. Lebedev Phys. Inst.* **36** 110 (2009); *Kratk. Soobshch. Fiz.* **36** (4) 26 (2009)
87. Burgin M S *Bull. Lebedev Phys. Inst.* **37** 280 (2010); *Kratk. Soobshch. Fiz.* **37** (9) 30 (2010)
88. Chluba J, Sunyaev R A *Astron. Astrophys.* **446** 39 (2006)
89. Kholupenko E E, Ivanchik A V *Astron. Lett.* **32** 795 (2006); *Pis'ma Astron. Zh.* **32** 883 (2006)
90. Grachev S I, Dubrovich V K *Astron. Lett.* **34** 439 (2008); *Pis'ma Astron. Zh.* **34** 483 (2008)
91. Burgin M S, Kauts V L, Shakhvorostova N N *Astron. Lett.* **32** 507 (2006); *Pis'ma Astron. Zh.* **32** 563 (2006)
92. Karshenboim S G, Ivanov V G *Astron. Lett.* **34** 289 (2008); *Pis'ma Astron. Zh.* **34** 323 (2008)
93. Kholupenko E E, Ivanchik A V, Varshalovich D A *Phys. Rev. D* **81** 083004 (2010)
94. Chluba J, Sunyaev R A *Mon. Not. R. Astron. Soc.* **402** 1221 (2010)
95. Henry R C *Astrophys. J.* **516** L49 (1999)